Biological production in the NE Pacific and its influence on air-sea CO_2 flux: Evidence from dissolved oxygen isotopes and O_2/Ar

L. W. Juranek,[1,2,3] P. D. Quay,[4] R. A. Feely,[2] D. Lockwood,[4] D. M. Karl,[5] and M. J. Church[5]

Received 13 July 2011; revised 27 March 2012; accepted 30 March 2012; published 15 May 2012.

[1] We determine rates of gross photosynthetic O_2 production (*GOP*) and net community O_2 production (*NCP*) using the triple oxygen isotope and O_2/Ar approach on two spring and two late summer meridional transects of the NE Pacific. Observed *GOP* and *NCP* in the subtropical (89 ± 9 and 8.3 ± 1.3 mmol O_2 m^{-2} d^{-1}, respectively) and subarctic (193 ± 16 and 16.3 ± 3.8 mmol O_2 m^{-2} d^{-1}) were in agreement with rates previously determined at time series stations in each region, validating the regional representativeness of these sites. At the transition zone chlorophyll front (TZCF), which migrates seasonally from 32°N in spring to 40°N in summer, *GOP* and *NCP* were elevated by 2–4× compared to adjacent areas. Coincident with the TZCF, increases in surface nitrate concentration and extensive changes in phytoplankton community composition were observed. HPLC pigment data indicated substantial increases in a prymnesiophyte (e.g., coccolithophore) biomarker at the TZCF on a spring and summer cruise, and a diatom biomarker on the spring cruise. Increases in remotely sensed surface particulate inorganic carbon concentration were also observed at the TZCF on all four cruises, indicating that coccolithophore production may contribute to increased productivity at the TZCF. Meridional trends in observed air-sea CO_2 flux on each cruise resembled those of the biologically induced CO_2 flux (*NCP*), but with an overprinting of the response of air-sea CO_2 exchange to summer warming. A simple carbon budget based on regional CO_2 flux climatology demonstrates the importance of *NCP* for net annual air-sea CO_2 uptake, although slow air-sea equilibration and seasonal solubility effects obscure this term.

Citation: Juranek, L. W., P. D. Quay, R. A. Feely, D. Lockwood, D. M. Karl, and M. J. Church (2012), Biological production in the NE Pacific and its influence on air-sea CO_2 flux: Evidence from dissolved oxygen isotopes and O_2/Ar, *J. Geophys. Res.*, *117*, C05022, doi:10.1029/2011JC007450.

1. Introduction

[2] The North Pacific is a diverse, dynamic basin that both participates in and responds to large-scale climate phenomena on a range of timescales [*Chavez et al.*, 2003; *Bond and Harrison*, 2000]. The region is also important for both natural and anthropogenic air-sea CO_2 exchange [*Gruber et al.*, 2009; *Takahashi et al.*, 2009]. A large fraction of the basin net annual CO_2 uptake results from a moderate air-sea flux (≈0.2–1 mol m^{-2} yr^{-1} [*Dore et al.*, 2003]) over the broad subtropical gyre region (approximately 15°–30°N). However, in the transition region between the subtropical and subarctic N. Pacific (approximately 30°–40°N), large ΔpCO_2 gradients drive a stronger CO_2 sink of 2 –3 mol C m^{-2} yr^{-1} [*Takahashi et al.*, 2009]. Both the marine solubility pump and biological pump are believed to play active roles in maintaining this strong CO_2 sink [e.g., *Takahashi et al.*, 2002; *Chierici et al.*, 2006; *McKinley et al.*, 2006], but a lack of biological rate observations in this remote region has made it difficult to quantify the role of biologically–regulated CO_2 flux and its potential vulnerability to future change.

[3] Observations at time series stations in the subtropical and subarctic N. Pacific have significantly enhanced our understanding of top-down and bottom-up controls on biological carbon cycling at these sites [e.g., *Karl*, 1999; *Karl et al.*, 2001; *Harrison*, 2002; *Whitney et al.*, 2005]. However, few field-based observations exist outside of these locations, and questions regarding the representativeness

[1]Joint Institute for the Study of the Atmosphere and Ocean, University of Washington, Seattle, Washington, USA.
[2]NOAA Pacific Marine Environmental Laboratory, Seattle, Washington, USA.
[3]Now at College of Earth, Ocean, and Atmospheric Sciences, Oregon State University, Corvallis, Oregon, USA.
[4]School of Oceanography, University of Washington, Seattle, Washington, USA.
[5]School of Ocean and Earth Science and Technology, University of Hawai'i at Mānoa, Honolulu, Hawaii, USA.

Corresponding author: L. W. Juranek, College of Earth, Ocean, and Atmospheric Sciences, Oregon State University, 104 CEOAS Administration Bldg., Corvallis, OR 97331-5503, USA. (laurie.juranek@noaa.gov)

0148-0227/12/2011JC007450

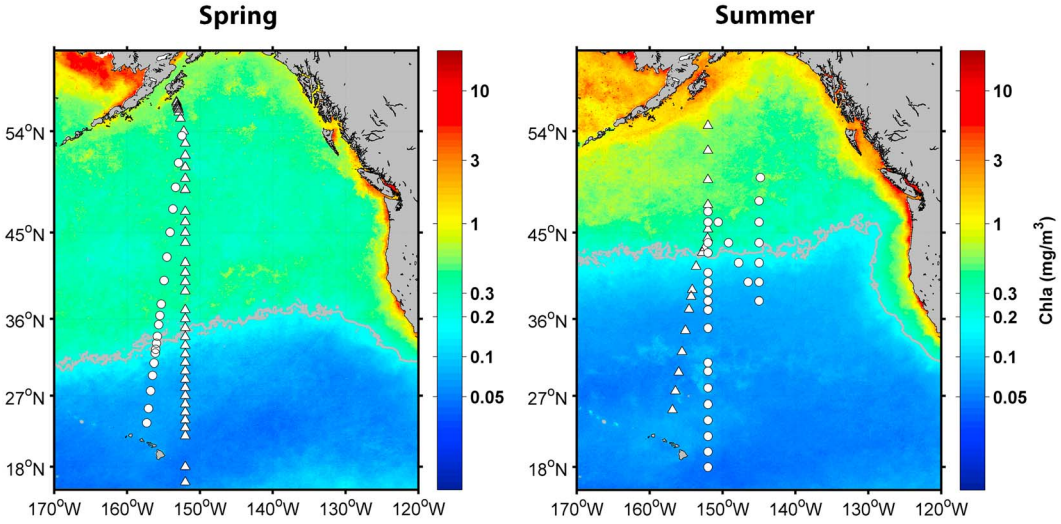

Figure 1. Climatology of SeaWiFS chl a for March and September with the position of the TZCF (0.2 mg m^{-3} chl a) shown with a gray line. Also shown are the sampling locations for two spring cruises (CB1, triangles; P16N, squares) and two summer cruises (CB2, triangles; STUD08, circles).

of time series data at the regional scale persist [*Boyd and Harrison*, 1999]. The need for basin-scale and global estimates of biological rate terms relevant to surface ocean CO_2 uptake, i.e., primary production and organic carbon export, requires the extrapolation of these geographically sparse time series data, despite little or no constraint on the resulting estimates throughout much of the surface ocean. Thus, there is a clear need for determination of biological rate terms throughout the N. Pacific basin to provide regional context for time series observations, to validate algorithms and models used to extrapolate limited field data to basin- and global scale [e.g., *Behrenfeld and Falkowski*, 1997; *Westberry et al.*, 2008; *Laws et al.*, 2000], and to better understand biological carbon cycling in historically undersampled areas.

[4] The ocean's biological pump is expected to respond to, and likely feedback on, future warming and carbon chemistry changes. While changes in physical supply rates might be easily modeled, complex and unexpected shifts in community structure might be equally important but are more difficult to predict. *Le Quere et al.* [2005] suggested that the failure to include a complex ecosystem response to climate may cause coupled climate models to underpredict the variability of future ocean CO_2 uptake. Efforts to include ecosystem-biogeochemistry feedbacks in climate models have been initiated [*Boyd and Doney*, 2002; *Le Quere et al.*, 2005] but progress and refinement is dependent on quantification of climate–ecosystem responses on a regional basis. Ecosystem responses have been looked at in some detail in the subtropical Pacific [*Karl et al.*, 2001; *Corno et al.*, 2007] and tight coupling between climate variability and higher trophic levels has been noted in the subarctic Pacific [*Mantua and Hare*, 2002; *Chavez et al.*, 2003], but a lack of data in the subtropical/subarctic transition leaves the linkages between larger-scale physical/chemical changes and biological responses in this important CO_2 sink region unresolved.

[5] From this discussion two questions which motivate this study emerge: (1) What is the role of the biological pump in net air-sea CO_2 exchange in the N. Pacific CO_2 sink region; and (2) what is the potential sensitivity of a biologically–regulated CO_2 sink to future climate forcing? Although both questions are difficult to answer unequivocally without decades of monitoring, we contribute to the discussion by introducing new biological rate and community composition data from meridional surveys of the N. Pacific basin, and use these data to elucidate potential mechanisms controlling biological carbon cycling in the N. Pacific CO_2 sink region. We use the triple oxygen isotopic composition of dissolved O_2 ($^{17}\Delta$ [*Luz and Barkan*, 2000, 2005; *Kaiser*, 2011]) and the dissolved O_2/Ar gas ratio to evaluate gross photosynthetic O_2 production (*GOP*), net community O_2 production (*NCP*), and the net/gross production ratio throughout the NE Pacific on four cruises (two spring, two late-summer, Figure 1). These data indicate that the subtropical–subarctic transition region, and specifically the transition zone chlorophyll (chl) front (TZCF [*Polovina et al.*, 2001]) is an area of enhanced biological production, export, and biologically–regulated CO_2 uptake. We also demonstrate the utility of the oxygen isotope and O_2/Ar approach for providing regional context for time series observations, improving spatial and temporal coverage of biological rate terms, and identifying the role of the ocean's biological pump in CO_2 uptake.

2. Setting

[6] Several contrasts are evident in the physical and biogeochemical settings of the subtropical and subarctic N. Pacific. Large-scale wind patterns, the NE Trade Winds and the Westerlies, set up an anticyclonic and cyclonic gyre circulation in the subtropical and subarctic regions, respectively [*Munk*, 1950]. Diffuse Ekman pumping (downwelling) helps to maintain a low nutrient, low chlorophyll (LNLC) condition in the subtropics, whereas Ekman suction (upwelling) helps maintain high surface macronutrient (e.g., NO_3^-) concentrations in the subarctic. Top-down grazing control and bottom-up micronutrient control likely both maintain the prevailing high nutrient, low chl (HNLC) condition of the subarctic region [*Harrison*, 2002].

[7] Multidecade time series observations of hydrography, pigments, nutrients, primary and new production have been established in the N. Pacific at several sites: in the subtropics at the Hawaii Ocean Time series (HOT) Station ALOHA (22.75°N, 158°W), and in the NE subarctic region at Ocean Station P (OSP: 50°N, 145°W). Time series observations are also available in the NW Pacific (e.g., station K2 at 47°N, 160°E), but we focus this discussion on the NE Pacific region. Observations at these time series stations have advanced our understanding of the mechanisms regulating marine biological pump function in the respective gyres, and have identified important differences between the two regions.

[8] In the subtropics, climate-driven changes in mixed layer (ML) depth and resulting changes in nutrient delivery are believed to drive changes in plankton community structure, effecting changes in biological production and export [*Karl et al.*, 2001; *Corno et al.*, 2007]. The dominant photautotrophs are the marine cyanobacteria *Prochloroccus* [*Karl et al.*, 2001], although several species of N_2-fixing cyanobacteria are believed to contribute substantially to primary and new production in summer months [*Karl et al.*, 1997; *Church et al.*, 2005]. Seasonality in hydrographic conditions and biological production is comparatively low, with an annual ML cycle that varies from ≈50 m during an enhanced stratification spring/summer season (April–October) to ≈80–100 m during a winter entrainment/mixing season (November–February) [*Brix et al.*, 2006; *Quay et al.*, 2010].

[9] The NE Pacific subarctic region is dominated by small cells <5 μm, with occasional contributions from larger cells >20 μm in summer [*Boyd and Harrison*, 1999]. The seasonal range in ML depth is comparable to that found in the subtropics, but spring shoaling is delayed by 1–2 months relative to the subtropics. Seasonality in biological production is greater than found in the subtropics, but compared to the subarctic gyre in the N. Atlantic, seasonality is slight; unlike the N. Atlantic there is no spring bloom, chl concentrations are relatively constant throughout all seasons, and there is only a three–fold range in primary productivity annually [*Welschmeyer et al.*, 1993; *Harrison*, 2002]. Light, stratification, and grazing seem to be the main controls on productivity by small phytoplankton, while the supply of the micronutrient iron limits growth of large cells [*Boyd and Harrison*, 1999]. Mesoscale variability is also an important feature of this gyre, with long–lived coastal origin Haida, Sitka, and Alaskan eddies driving enhanced biological production via delivery of shelf–derived iron [*Whitney et al.*, 2005]. Climate variability effects on fish populations and zooplankton stocks have been well-documented [*Mantua and Hare*, 2002; *Chavez et al.*, 2003], but links to lower trophic levels have not been established.

[10] The transition region between the subtropical and subarctic gyres (32°N–42°N) is a region of comparatively weak surface winds, and strong gradients in surface temperature and salinity [*Roden*, 1991]. Differential wind stress (decreasing northward in the subtropics and southward in the subarctic) results in areas of convergence at the subtropical (31°–34°N) and subarctic (40°N–43°N) frontal zones, while weak stress in the region between results in a broad region of confluence (i.e., water transported from northern and southern regions comes together without implied vertical motion [*Roden*, 1980, 1991]). The northern extent of the transition zone is characterized by the disappearance of the subarctic halocline, which results in a stability "gap" between 37°N and 43°N during the non-stratified winter season [*Roden*, 1991]. The southern boundary of the transition zone is marked by strong surface salinity fronts which delineate the northward extent of warmer, saltier subtropical water.

[11] Superimposed on the transition zone physical setting is a basin–wide biological feature, the TZCF [*Polovina et al.*, 2001]. Typically defined as the 0.2 mg m^{-3} surface chl contour, the location of the TZCF varies seasonally from a southernmost position of 30°N in winter to a northernmost location of 42°N in summer (Figure 1). The migratory pathways of albacore tuna and loggerhead turtles coincide with the TZCF position seasonally; it is thought that convergence and aggregation of secondary production at the TZCF provides an important food source [*Polovina et al.*, 2001]. Several studies have suggested that variation in ML depth (and resulting impacts on surface nutrient delivery) is a primary determinant of TZCF excursions from climatological means in ecosystem models [*Glover et al.*, 1994; *Polovina et al.*, 1995; *Chai et al.*, 2003]. However, *Ayers and Lozier* [2010] suggested that the seasonal migration of the TZCF could not be explained by ML depth seasonality (and attendant vertical fluxes) because the subtropical nitricline is always deeper than the winter ML. They proposed that seasonal front migration is a result of increased surface wind stress in winter, which results in enhanced surface Ekman transport of NO_3^- from the subarctic to the transition region. Under reduced summer wind stress, the TZCF relaxes back to the gyre-gyre boundary at ≈40°N.

[12] An oceanic sink for CO_2 is found over the majority of the N. Pacific basin, but reaches a maximum over 30°–40°N, 120°E–120°W [*Takahashi et al.*, 2009], an area that corresponds to the transition region physical and biological fronts described above. Seasonal and interannual controls on this air-sea CO_2 sink have been scrutinized in a number of observational and modeling studies [*Takahashi et al.*, 2002; *Chierici et al.*, 2006; *McKinley et al.*, 2006; *Ayers and Lozier*, 2012], and it is generally recognized that the solubility pump and biological pump both play important roles in this region. However, changes in surface pCO_2 not related to temperature (e.g., "non–T effects"), which include both biological CO_2 uptake and addition/removal of dissolved inorganic carbon (DIC) via vertical and horizontal transport, are often grouped together in these studies. Lack of independent constraint on biological CO_2 uptake leaves the relative importance of the solubility versus biological pump in this region somewhat unresolved. In addition, while global coupled models are generally able to simulate responses of surface water pCO_2 and air-sea CO_2 flux to changes in the physical setting, controls such as biological drawdown are much harder to simulate [*McKinley et al.*, 2006]. Given the importance of biological CO_2 uptake and the lack of historical data in this dynamic, remote region, we used the $^{17}\Delta$ and O_2/Ar approach to evaluate regional trends in important biological rate terms *GOP* and *NCP*.

3. Methods

3.1. Triple Oxygen Isotope and O_2/Ar Approach

[13] In this study we use the triple oxygen isotope approach to determine *GOP* and the dissolved O_2/Ar gas ratio approach to determine *NCP*. The oxygen isotope method and

its application has been discussed in detail elsewhere [*Luz and Barkan*, 2000, 2005; *Hendricks et al.*, 2004, 2005; *Juranek and Quay*, 2005; *Reuer et al.*, 2007], and some aspects of its use are rapidly evolving [*Kaiser*, 2011; *Nicholson*, 2011; *Prokopenko et al.*, 2011; *Luz and Barkan*, 2011], but we briefly recap major points here. The method utilizes a unique isotopic signature of O_2 generated by stratospheric photochemical reactions involving O_3, O_2, and CO_2 [e.g., *Lämmerzahl et al.*, 2002]. When normalized for differences in the $^{18}O/^{16}O$ ratio, these reactions produce atmospheric O_2 that has a low ^{17}O ("^{17}O deficit") relative to O_2 produced photosynthetically [*Helman et al.*, 2005; *Eisenstadt et al.*, 2010; *Luz and Barkan*, 2011]. Thus, relative to air O_2, O_2 derived from marine photosynthesis can be considered to have a ^{17}O-excess. Using an O_2 and oxygen isotope mass balance approach, the ML average *GOP* (mmol O_2 m^{-2} d^{-1}) can be estimated from measurements of the ^{17}O-excess if an estimate of the air–sea gas transfer rate of O_2 is supplied by a wind speed based parameterization [e.g., *Nightingale et al.*, 2000; *Ho et al.*, 2006; *Sweeney et al.*, 2007].

[14] The ^{17}O-excess ($^{17}\Delta$) can be quantified as follows [*Luz and Barkan*, 2005, 2011; *Kaiser*, 2011]:

$$^{17}\Delta = 10^6\left[\ln\left(10^{-3}\delta^{17}O+1\right)-\lambda\ln\left(10^{-3}\delta^{18}O+1\right)\right], \quad (1)$$

where $\delta^{17}O$ and $\delta^{18}O$ are given in per mil (‰) using standard delta notation, $\delta^x O = 10^3\left[\frac{\left({}^xO/{}_{16}O\right)_{sample}}{\left({}^xO/{}_{16}O\right)_{reference}}-1\right]$, x = 17 or 18, and the reference of choice is air O_2.The range in $^{17}\Delta$ of dissolved O_2 ($^{17}\Delta_{diss}$) in the ocean is small, 0.000 to 0.250‰, and is typically reported in units of per meg (1 per meg = 0.001‰). The appropriate slope (λ) depends on the processes influencing the isotopic composition of O_2 [*Luz and Barkan*, 2005, 2011; *Kaiser*, 2011; *Nicholson*, 2011], but for studies of marine photosynthesis, λ should be 0.518 [e.g., *Angert et al.*, 2003; *Luz and Barkan*, 2005, 2011]. This choice of λ causes respiration to have no effect on $^{17}\Delta$, since the respiratory isotope effect for $\delta^{17}O$ relative to $\delta^{18}O$ is also 0.518. Marine photosynthetic O_2 ($^{17}\Delta_p$) has a value close to that of seawater, experimentally determined to be ≈250 per meg [*Luz and Barkan*, 2000, 2011]. Dissolution of O_2 in seawater imparts a small, positive $^{17}\Delta$ signature ($^{17}\Delta_{eq}$); however, the value is currently debated, with several studies [*Luz and Barkan*, 2000; *Sarma et al.*, 2006; *Juranek and Quay*, 2005] reporting a value of 16 per meg, and others [*Reuer et al.*, 2007; *Stanley et al.*, 2010] reporting a value of 8 per meg (see also *Kaiser* [2011] for a summary of all $^{17}\Delta_{eq}$ experiments). For the purposes of our discussion, we adopt the more recent estimates of *Luz and Barkan* [2009], who found $^{17}\Delta_{eq}$ to range from 4 to 17 per meg as a function of temperature, $^{17}\Delta_{eq}$ = 0.6(T) + 1.8 (where T is in °C), because the results are partially consistent with all studies and show improved reproducibility. We discuss the potential errors and biases imparted by this choice in section 3.5. Values calculated using a constant value of 8 per meg are available in the auxiliary material.[1]

[15] The O_2 budget of the ML can be described as

$$h\frac{\partial[O_2]}{\partial t} = GOP - R + k_{O2}\left([O_2]_{eq}-[O_2]\right) + K_z\frac{\partial[O_2]}{\partial z} + h\nabla\cdot\bar{u}[O_2], \quad (2)$$

where *GOP* is as previously defined, R is the respiration rate, the third term is the rate of air–sea O_2 exchange, and the fourth and fifth terms are expressions for diffusive and advective (meridional and zonal) O_2 transports, respectively. The air–sea O_2 gas transfer term includes the gas–transfer coefficient for O_2 (k_{O2}) and $[O_2]_{eq}$, the equilibrium $[O_2]$ at in situ temperature and salinity. All terms in equation (2) represent O_2 fluxes in mmol m^{-2} d^{-1}. Analogous expressions can be constructed for O_2 isotopomers ($^{18}O^{16}O$ and $^{17}O^{16}O$), taking into account appropriate isotopic ratios, and equilibrium and kinetic isotope fractionation effects [see *Hendricks et al.*, 2004, appendix; *Kaiser*, 2011; *Prokopenko et al.*, 2011]. Because observations are often time and space limited, and the physical supply of O_2 is often of second order importance relative to gas exchange and production/consumption terms during spring–summer in open ocean regimes [e.g., *Emerson et al.*, 2008], the O_2 transports (fourth and fifth terms in equation (2)) are frequently neglected and steady state $\left(\frac{\partial[O_2]}{\partial t}=0\right)$ assumed.

[16] Several methods have been presented for determining *GOP* from observations of $^{17}\Delta$ using an O_2 mass balance (we refer the reader to *Kaiser* [2011] for an excellent summary). The most familiar is the original method introduced by *Luz and Barkan* [2000], which neglects transport terms and assumes steady state, as discussed above

$$\frac{GOP}{k_{O2}[O_2]_{eq}} = \frac{^{17}\Delta_{diss} - {}^{17}\Delta_{eq}}{^{17}\Delta_p - {}^{17}\Delta_{diss}}. \quad (3)$$

[17] Recently, *Kaiser* [2011] and *Prokopenko et al.* [2011] independently introduced improved equations for determining *GOP* using inputs of $\delta^{17}O$ and $\delta^{18}O$ ($^{17}\Delta$ is not used explicitly, although the ^{17}O-excess identified by $^{17}\Delta$ is still an important constraint). These "dual-delta" methods remove certain implicit assumptions and approximations which previously led to potential biases in *GOP*. We reproduce the *Prokopenko et al.* [2011] equation here

$$\frac{GOP}{k_{O2}[O_2]_{eq}} = \left(\frac{\left(1-\frac{10^{-3}\delta^{17}O_{eq}+1}{10^{-3}\delta^{17}O_{diss}+1}\right)-\lambda\left(1-\frac{10^{-3}\delta^{18}O_{eq}+1}{10^{-3}\delta^{18}O_{diss}+1}\right)}{\left(\frac{10^{-3}\delta^{17}O_{p}+1}{10^{-3}\delta^{17}O_{diss}+1}-1\right)-\lambda\left(\frac{10^{-3}\delta^{18}O_{p}+1}{10^{-3}\delta^{18}O_{diss}+1}-1\right)}\right). \quad (4)$$

[18] Values of $\delta^{17}O$ and $\delta^{18}O$ corresponding to air-sea O_2 equilibrium (*eq*), and photosynthetic O_2 production (*p*) are supplied as constants, and observed values of $\delta^{17}O$ and $\delta^{18}O$ of dissolved O_2 (*diss*) are used to solve for the fraction of mixed layer O_2 arising from photosynthetic production (*GOP*) relative to that arising from air-sea gas exchange ($k_{O2}[O_2]_{eq}$). We use equation (4) to calculate *GOP* in this study (values calculated from the method given by *Kaiser* [2011] are within 5%, and are available in the auxiliary material), but will continue to refer to $^{17}\Delta_{diss}$ throughout our discussion, as it is a much more intuitive tracer of ML O_2 of biological origin than the individual $\delta^{17}O$ and $\delta^{18}O$ values.

[1]Auxiliary materials are available in the HTML. doi:10.1029/2011JC007450.

Because the choice of constants (λ, $\delta^{17}O_p$, $\delta^{18}O_p$, $\delta^{17}O_{eq}$, $\delta^{18}O_{eq}$, or $^{17}\Delta$ equivalents) and the assumed model (e.g., equation (3) versus equation (4)) can implicitly bias results, several have suggested that all reported *GOP* values should also be accompanied by $\delta^{17}O_{diss}$ and $\delta^{18}O_{diss}$ data and assumed constants so that individual studies can be directly intercomparable [e.g., *Kaiser*, 2011; *Nicholson*, 2011; *Prokopenko et al.*, 2011]. Following this recommendation, all isotope data and constants are provided in the auxiliary material.

[19] The rate of net community production (*NCP*), i.e, the net O_2 difference between *GOP* and community respiration, *R*, can be determined in situ with measurements of the dissolved O_2/Ar gas ratio. The inert tracer gas Ar is useful because Ar behaves as a biologically–inert analog to O_2 — that is, it behaves similarly to O_2 with respect to solubility–induced changes in saturation, but has no biological sources or sinks. The measured $([O_2]/[Ar])_{meas}$, divided by the ratio expected at solubility equilibrium, $([O_2]/[Ar])_{eq}$, provides a measure of the biologically–induced change to O_2 saturation ($\Delta O_2/Ar$) if Ar is assumed to be in equilibrium with the atmosphere. If steady state is assumed, *NCP* can be estimated from $\Delta O_2/Ar$ as follows [*Craig and Hayward*, 1987; *Emerson et al.*, 1991, 1997; *Hendricks et al.*, 2005; *Kaiser et al.*, 2005]:

$$NCP = k_{O2}[O_2]_{eq}(\Delta O_2/Ar - 1). \quad (5)$$

[20] *NCP* can be thought of as organic carbon export potential: this is the net organic carbon production (inferred from O_2 excess) that is available for transfer to higher trophic levels or transport out of the ML, whether by a sinking flux or physical transport. When $\Delta O_2/Ar$ and $^{17}\Delta_{diss}$ measurements are combined, the *NCP*/*GOP* ratio, equivalent to an e-ratio [*Laws et al.*, 2000] in O_2 currency, can be determined.

3.2. Sample Collection and Analysis

[21] Dissolved gas samples were collected on four cruises in the NE Pacific (Figure 1): two ship relocation transits between Honolulu, HI and Kodiak, AK on the *R/V Kilo Moana* (8–15 April 2003 and 2–9 October 2003, COOKBOOK 1 and 2, respectively, hereafter CB1 and CB2), and two hydrographic cruises on the *Thomas G. Thompson* along 152°W (12–30 March 2006 and 28 August to 18 September 2008, CLIVAR P16N and UW Student cruise, respectively, hereafter P16N and STUD08). Samples were collected by Niskin-style water samplers in the surface ML during standard conductivity-temperature-depth casts, primarily at depths of 10–15 m, using the dissolved gas sampling protocols described in *Emerson et al.* [1999]. Occasionally, an additional 4–6 samples were taken from depths between 15 and 250 m. One surface sample was also collected from the underway seawater supply line during CB2 when adverse weather prevented normal sampling.

[22] Prior to isotopic analysis, samples were prepped by cryogenic removal of H_2O and CO_2 and chromatographic separation of N_2 from the dissolved gas mixture [*Juranek and Quay*, 2005]. The $\delta^{17}O$ and $\delta^{18}O$ of the extracted gas mixture was analyzed on a Finnigan MAT 251 (CB1, CB2, P16N) or a Thermo MAT 253 (STUD08) isotope ratio mass spectrometer via simultaneous collection of m/z 32, 33, and 34 from 75 paired determinations of the gas mixture versus an internal reference standard; typical internal precision (standard error of mean = $\frac{\sigma}{\sqrt{n}}$) for each measurement was 0.007 ‰, 0.003 ‰, and 7 per meg for $\delta^{17}O$, $\delta^{18}O$, and $^{17}\Delta$ respectively. Repeat measurements of air run daily with samples carried a between–sample standard error of 0.003 ‰, 0.005 ‰, and 1.4 per meg for $\delta^{17}O$, $\delta^{18}O$, and $^{17}\Delta$, respectively (n ≈ 25 for each set of samples). All $\delta^{17}O$, $\delta^{18}O$, and $^{17}\Delta$ values are reported relative to an air standard.

[23] The $([O_2]/[Ar])_{meas}$ ratio was determined by peak jumping of m/z 32 and 40 after the $\delta^{17}O$ and $\delta^{18}O$ determination, with a typical precision of ±3‰ (0.3%) based on repeated measurements of the air standard. The $([O_2]/[Ar])_{eq}$ was calculated using the O_2 and Ar solubility equations of *García and Gordon* [1992] and *Hamme and Emerson* [2004], respectively.

3.3. Determination of k_{O2}

[24] To determine k_{O2} we used the wind–speed based parameterization of *Ho et al.* [2006], which predicts gas transfer coefficients that are in close agreement with recently published relationships for both purposeful tracer experiments [e.g., *Nightingale et al.*, 2000] and a recently recalculated inversion of the ^{14}C bomb inventory [*Sweeney et al.*, 2007]. The average wind speed used to calculate k_{O2} for each sampling location was determined from remotely–sensed QuikSCAT winds (0.25° gridded global resolution), downloaded from the NASA Jet Propulsion Lab Physical Oceanography Distributed Active Archive Center (http://podaac.jpl.nasa.gov). To account for time-varying k_{O2} over the approximate two week residence time of dissolved O_2 with respect to gas exchange (i.e., $\tau = z_{ML}/k_{O2}$, with z_{ML} the ML depth), we used the approach described by *Reuer et al.* [2007], in which daily k_{O2} values are weighted by the fraction of the ML ventilated on preceding days, and the weighted average is computed from 60 days of wind observations prior to sampling. The z_{ML} was determined for each sample location using cast conductivity, temperature, and depth data and a density criterion of a 0.125 kg m^{-3} difference from the surface [*Monterey and Levitus*, 1997].

3.4. Ancillary Data

[25] Ancillary data sets useful for our analysis of factors controlling *GOP* and *NCP* rate variability were obtained from various sources. For April and October 2003 CB1 and CB2 cruises, nutrient, pigment, phytoplankton community structure, dissolved inorganic carbon (DIC), and total alkalinity (TA) concentrations were determined by the University of Hawaii Microbiological group (using protocols employed at the HOT site) and were downloaded from http://hahana.soest.hawaii.edu/cookbook/. For the March 2006 P16N cruise, nutrient, DIC, and TA were determined as part of the core CLIVAR hydrography and analyzed according to WOCE/CLIVAR protocols (http://cchdo.ucsd.edu/). Chl a concentration for P16N was determined fluorometrically (N. Nelson, UCSB, personal communication, 2010). For the September 2008, STUD08 cruise, nutrient data were determined using WOCE protocols on a Technicon AAII system and DIC and TA were determined by the NOAA–PMEL CO_2 group using best practices outlined in *Dickson et al.* [2007]. Chl for STUD08 was determined fluorometrically (M. Kavanaugh, OSU, personal communication, 2010).

[26] We also made use of several remotely sensed parameters in our analysis. For each cruise, gridded 9km, 8–day composite averages of SeaWiFS chl concentration and MODIS particulate inorganic carbon (PIC) [*Balch et al.*, 2005] were downloaded from http://oceancolor.gsfc.nasa.gov for timeframes corresponding to sample collection. To derive surface Ekman transports, we used directional components of wind speed from QuikSCAT (http://podaac.jpl.nasa.gov) to calculate zonal and meridional wind stress, τ_x and τ_y. Horizontal Ekman transports were calculated as $u_{Ek} = \tau_y/\rho f$ and $v_{Ek} = \tau_x/\rho f$, where ρ and f are density and the Coriolis parameter, respectively. Daily u_{Ek} and v_{Ek} for 30 days prior to the cruise start date were averaged to determine surface transports for each cruise.

3.5. Analytical and Model Based Uncertainties for $^{17}\Delta$- and $\Delta O_2/Ar$-Derived Rates

[27] Limits to analytical precision contribute ≈15–30% uncertainty to individual *GOP* rates, depending on the magnitude of ^{17}O excess ($^{17}\Delta_{diss}$) [*Juranek and Quay*, 2010]. The variable uncertainty is a function of the signal-to-noise ratio; the noise level is reasonably fixed for any given measurement (±7 per meg, the typical uncertainty of individual $^{17}\Delta_{diss}$ observations) and the productivity signal, $^{17}\Delta_{diss} - {}^{17}\Delta_{eq}$, is variable (e.g., typically 10–60 per meg for most open ocean conditions). Thus, the *GOP* rate calculated from $^{17}\Delta_{diss}$ = 30 per meg will have a higher proportional error than the *GOP* rate calculated from $^{17}\Delta_{diss}$ = 60 per meg. *GOP* rates based on several $^{17}\Delta_{diss}$ determinations are better constrained than individual estimates, since the mean value is typically known better than ±7 per meg.

[28] Additional uncertainty in *GOP* rate estimates is contributed from other model terms. Uncertainty in the gas transfer coefficient k_{O2} (taken as twice the spread in k_{O2} values predicted by the *Nightingale et al.* [2000], *Ho et al.* [2006], and *Sweeney et al.* [2007] parameterizations) directly propagates to a ± 15% uncertainty in the calculated *GOP*. Uncertainties in $^{17}\Delta_p$ and $^{17}\Delta_{eq}$ (or $\delta^{17}O$ and $\delta^{18}O$ components, for equation (4)) also contribute: assuming a ±15 per meg and ± 3 per meg, uncertainty for $^{17}\Delta_p$ and $^{17}\Delta_{eq}$, respectively [*Luz and Barkan*, 2000, 2009, 2011], total uncertainty for *GOP* rates calculated in this study ranged from 20 to 100%, with a median of 35% (see Table S1 in Text S1 for individual uncertainties). Adopting a $^{17}\Delta_{eq}$ = 8 per meg for all temperatures (see section 3.1) would result in systematically higher *GOP* for most of the samples reported here (median relative difference: 10%; see Table S2 in Text S1 for comparison of values calculated with $^{17}\Delta_{eq}$ = 8 per meg and those reported here).

[29] Because the analytical uncertainty for $([O_2]/[Ar])_{meas}$ is small (0.3%), when $\Delta O_2/Ar$ is significantly different from 1.0, uncertainty in the *NCP* calculated by equation (5) approaches the uncertainty for the determination of k_{O2} alone (±15%). As $\Delta O_2/Ar$ approaches equilibrium (i.e., $([O_2]/[Ar])_{meas} = ([O_2]/[Ar])_{eq}$, $\Delta O_2/Ar = 1$), uncertainties can inflate to ±100%. In this study, *NCP* uncertainty ranged from 15 to 100%, with a median of 26% (Table S1 in Text S1).

[30] Neglect of the mixing and advection terms in the ML O_2 budget (equation (2)) can also result in potential biases in ML *GOP* and *NCP* estimates. In areas where the photic layer depth exceeds z_{ML}, fall entrainment of waters from beneath the ML with elevated $^{17}\Delta_{diss}$ and $\Delta O_2/Ar$ can cause an overestimate in calculated *GOP* and *NCP* if not explicitly accounted for [*Emerson et al.*, 2008; *Quay et al.*, 2010]. Similarly, in stratified summer periods, diffusive mixing of high $^{17}\Delta_{diss}$ and $\Delta O_2/Ar$ from sub ML waters could enhance ML $^{17}\Delta_{diss}$ and $\Delta O_2/Ar$ signals. Diffuse Ekman pumping/suction could also induce positive or negative biases to the ML O_2 budget depending on season. Recently, *Nicholson et al.* [2012] evaluated entrainment and mixing effects on surface ML $^{17}\Delta_{diss}$ in the subtropical Pacific at Station ALOHA using a 1-D upper ocean model. They found these processes could bias ML $^{17}\Delta_{diss}$ significantly throughout the year; largest biases in calculated *GOP* occurred in fall (October–December) and were attributed to entrainment (48 mmol O_2 m^{-2} d^{-1} difference between modeling scenarios, or ∼70% of their calculated productivity) and smallest biases in calculated *GOP* occurred in spring (April–June) during ML shoaling (26 mmol m^{-2} d^{-1} bias, or 42% of modeled productivity). Similar evaluation of the mixing/entrainment bias on *NCP* on a seasonal basis has not been reported, although *Emerson et al.* [2008] found entrainment to be one of the smallest terms in the O_2 mass balance used to constrain *NCP* at Station ALOHA, and *Hamme and Emerson* [2006] determined that an order of magnitude range in diapycnal diffusivity (10^{-4} to 10^{-5}) in 1-D model runs similar to those performed by *Nicholson et al.* [2012] did not influence the organic carbon production calculated in the ML on an annual basis. Unfortunately, $^{17}\Delta_{diss}$ modeling results are not available for the subarctic NE Pacific, and although the annual cycle of O_2 has been modeled at OSP [*Steiner et al.*, 2007], sensitivity of the modeled biological production to physical terms was not described.

[31] Obviously, fully accounting for all dynamical biases on ML $^{17}\Delta_{diss}$ and $\Delta O_2/Ar$ using observations that are adequately resolved in both space and time would be preferred. However, this approach is not always practical or logistically feasible, as is the case with the regional-scale opportunistic surveys presented here. Therefore, we do not attempt to correct for mixing biases, but are mindful of the potential caveats in our discussion.

3.6. Conversion of GOP and NCP to Carbon-Based Equivalents

[32] One drawback of *GOP* and *NCP* rates determined from an O_2 budget approach is that the rates are in O_2, rather than C-based currency, and conversion between the quantities is not always straightforward. Even aside from the obvious time and space scale differences, $^{17}\Delta$–based *GOP* rate is an entirely different rate term than that measured by the more commonly used ^{14}C–incubations, which many consider an estimate of NPP [e.g., *Marra and Barber*, 2004]. In order to compare our $^{17}\Delta$–based *GOP* to the larger, historical database of ^{14}C–based measurements, we used an empirical relationship derived from ^{18}O–labeled and ^{14}C–labeled 24 h bottle incubations during JGOFS process studies in the Equatorial Pacific, Arabian Sea, North Atlantic, and Southern Ocean [i.e., *GOP* = 2.7(24-h ^{14}C–incubation experiment), where GOP and ^{14}C-NPP are given in mmol m^{-3} d^{-1} of O_2 and C, respectively [see *Marra*, 2002; *Hendricks et al.*, 2005; *Reuer et al.*, 2007; *Juranek and Quay*, 2010]. Therefore, *GOP*/2.7 gives an approximation of a ^{14}C-NPP equivalent. Although empirically determined,

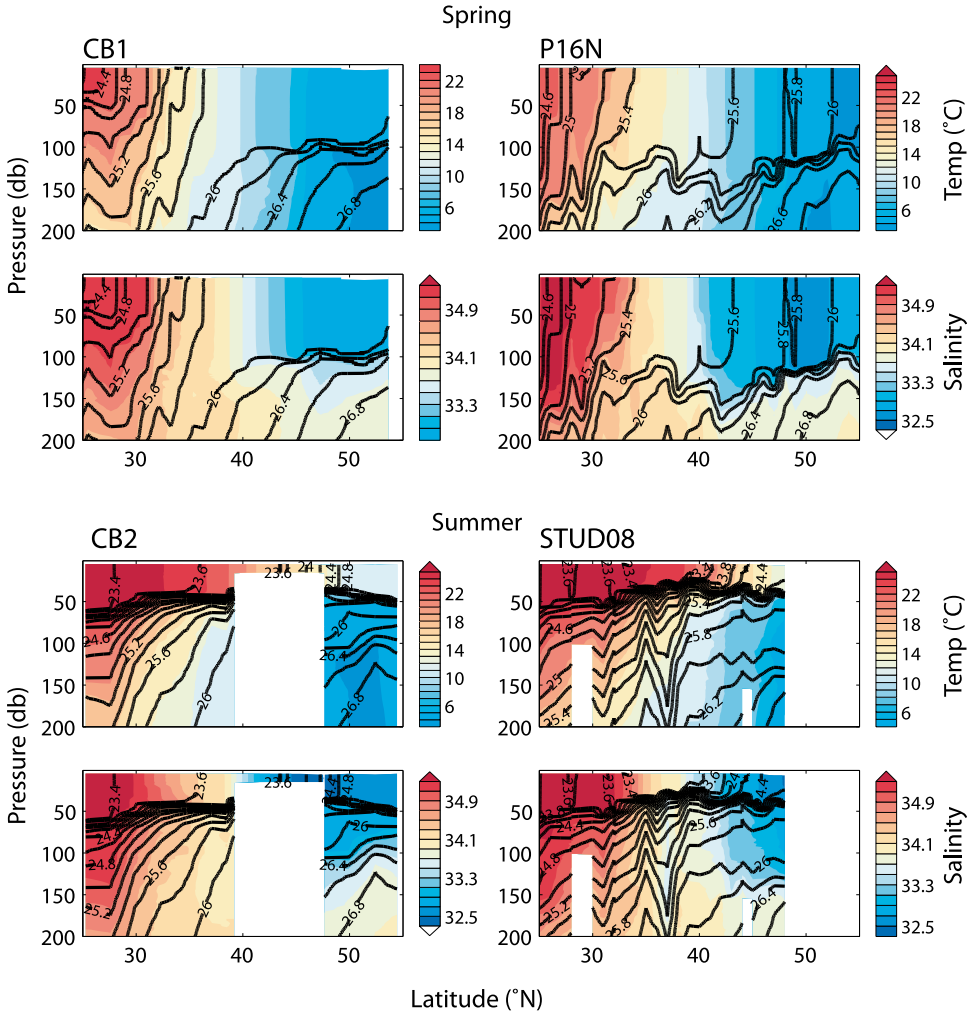

Figure 2. Hydrographic conditions for the four meridional surveys. Shown are temperature and salinity (colors) overlaid with density contours at 0.2 kg m^{-3} intervals. Adverse weather prohibited hydrographic casts between 40°N and 47°N during CB2; underway seawater temperature and salinity was used to plot surface trends over this interval.

the 2.7 factor is consistent with estimates of photosynthetic quotients relating O_2 production to C production, Mehler and photorespiration effects, and the recycling of labeled $PO^{14}C$ over the course of the incubation [*Juranek and Quay*, 2010]. We also note that a recent estimate of chl-specific GOP:NPP determined from chemostat cultures is similar (i.e., 3.3 [*Halsey et al.*, 2010]). In practice this ratio is likely much more variable than is assumed here, and several previous studies have noted that in situ $^{17}\Delta$–based *GOP* in the ML is often more than 2.7 times ML-integrated ^{14}C-based NPP [e.g., *Luz and Barkan*, 2009; *Nicholson et al.*, 2012], particularly under bloom-type conditions, which may indicate potential biases in the in situ $^{17}\Delta$ approach, incubation based ^{14}C approach, and/or difference in spatial/temporal averaging inherent to bottle and tracer-based approaches [*Juranek and Quay*, 2005; *Quay et al.*, 2010]. However, because there is no absolute standard for productivity measurements, and comparisons between various methods are instructive for evaluating potential biases, the 2.7 scaling factor is used in section 4.3 to provide a useful framework for intercomparisons between ^{14}C– NPP and $^{17}\Delta$– *GOP* estimates.

[33] To compare O_2–based *NCP* and *NCP*/*GOP* ratios to historical carbon-based measurements we followed the approach of *Hendricks et al.* [2005]. O_2–based *NCP* was converted to a comparable carbon flux using a photosynthetic quotient of 1.4 for new, "export" production [*Laws*, 1991]. *NCP*/*GOP* was converted to a carbon-based export ratio (e-ratio [*Laws et al.*, 2000]), comparable to the more traditional f-ratio [e.g., *Eppley and Peterson*, 1979], using the factor 2.7/1.4 to convert *GOP* to NPP and *NCP* to a carbon currency, i.e., $\frac{NCP(O_2)/1.4}{GOP/2.7} = \frac{NCP(C)}{^{14}C-NPP} \equiv$ e-ratio.

4. Results and Discussion

4.1. Overview of NE Pacific Productivity Trends

[34] The four NE Pacific cruises reveal significant regional and seasonal scale variability in upper ocean properties relevant to biological carbon cycling (Figures 2 and 3). To streamline discussion of the results, we present observations grouped by season (spring: April 2003 and March 2006 results of CB1 and P16N, respectively; late-summer/early

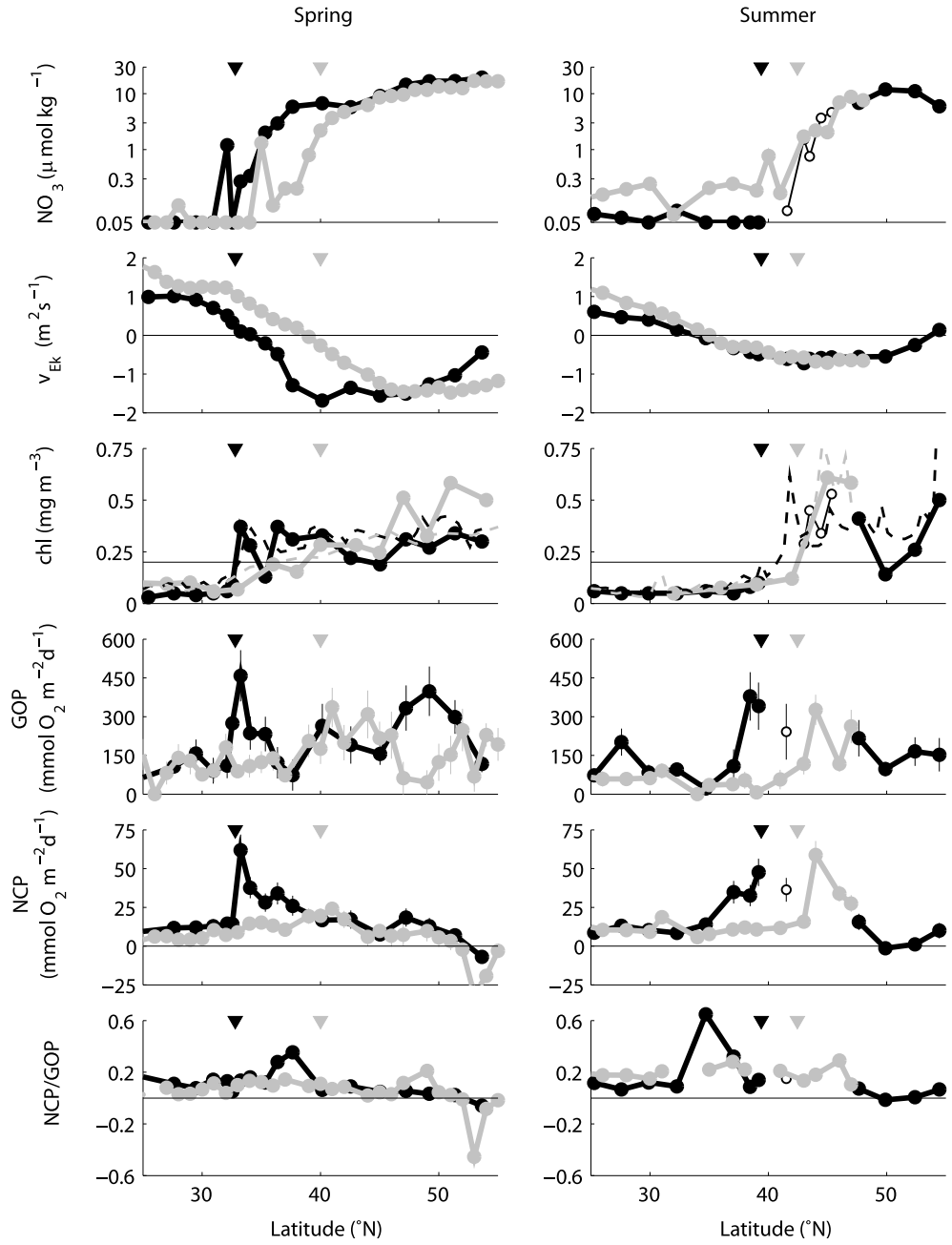

Figure 3. Meridional trends in surface properties relevant to biological production. (left) Trends for two spring cruises CB1 (black) and P16N (gray). (right) Trends for two summer cruises CB2 (black) and STUD08 (gray), unfilled circles between 40°N and 47°N designate samples collected from the underway seawater supply during adverse weather. Inverted triangles at the top of each figure indicate approximate position of the TZCF for each cruise. Shown are trends for surface NO_3^- (for CB1 and CB2, N + N), meridional Ekman transport derived from QuikSCAT winds (v_{Ek}), chl a (solid lines are discrete samples, dotted lines are 8-day averages from SeaWiFS, thin horizontal line indicates 0.2 mg m^{-3}), *GOP*, *NCP*, and *NCP/GOP*. Error bars for *GOP* and *NCP* data points are calculated from the propagated uncertainty in mean $^{17}\Delta_{diss}$ or $\Delta O_2/Ar$ (standard error of mean of all ML samples at a given station), as well as uncertainties in other model terms from equations (3) and (5) (see text and Table S1 in Text S1).

fall: October 2003 and September 2008 results of CB2 and STUD08 cruises, respectively). The October and September results are classified as late-summer/early fall rather than "fall" because of the strong stratification and shallow ML depths observed throughout the basin on both of these cruises (Figure 2). Spatial variability in observations is discussed in terms of regions: subtropical, transition, and subarctic, with regions defined according to the position of the subtropical front (i.e., the surface outcropping of the 34.8 isohaline) and the subarctic front (i.e., the surface outcropping of the

33.8 isohaline) [*Roden*, 1980, 1991]. Observations north and south of the subarctic/subtropical fronts were categorized as subarctic and subtropical, respectively, while those between were categorized as transitional. Data collected within $\pm 1^\circ$ latitude of the 0.2 mg m^{-3} surface chl horizon were also categorized as "TZCF." Exact boundaries for each cruise are given in Table 1.

[35] In the spring, the TZCF was at the same approximate latitude as the zero-crossing of northward and southward meridional Ekman transport (v_{Ek}) and the appearance of NO_3^- (or for CB1, $NO_3^- + NO_2^-$, hereafter N+N) greater than 0.3 μmol kg^{-1} in surface waters (Figure 3). Coincident with the chl, nutrient, and Ekman fronts, *GOP* and *NCP* rates also increased; the CB1 increase was substantial, with TZCF *GOP* and *NCP* averages of 323 $\pm$ 69 and 37.9 $\pm$ 13.8 mmol m^{-2} d^{-1} (mean $\pm \frac{\sigma}{\sqrt{n}}$), respectively, compared to subtropical region averages of 100 $\pm$ 24 and 11.2 $\pm$ 1.0 mmol m^{-2} d^{-1} (Figure 3 and Table 1). The TZCF *GOP* and *NCP* increases during P16N were more moderate, but rates (239 $\pm$ 49 and 20.9 $\pm$ 1.6 mmol m^{-2} d^{-1} for *GOP* and *NCP*, respectively) were still significantly higher than in the subtropics (94 $\pm$ 16 and 4.0 $\pm$ 2.4, Table 1). Some interannual variability in the location of the TZCF and v_{Ek} convergence during early spring is evident in the April 2003 (CB1) and March 2006 (P16N) data, with the 2006 front location much further northward than usual (Figures 1 and 3) [see also *Ayers and Lozier*, 2010].

[36] Overall, regional *GOP* and *NCP* averages from both spring cruises were highest for the TZCF (281 $\pm$ 38 and 29.4 $\pm$ 6.6 mmol m^{-2} d^{-1}, respectively, Table 1). Regional *GOP* was similar in the subarctic and transition regions in spring (188 to 199 mmol m^{-2} d^{-1}), and subtropical region *GOP* was lower by a factor of 2 (96 mmol m^{-2} d^{-1}, Table 1). Regional averages of *NCP* did not follow the same pattern; subarctic region *NCP* was lowest (2.8 $\pm$ 3.0 mmol m^{-2} d^{-1}), subtropical region *NCP* was slightly higher (6.0 $\pm$ 1.9 mmol m^{-2} d^{-1}), and transition region *NCP* was 3.5$\times$ the subtropical region spring average (21.2 $\pm$ 3.0 mmol m^{-2} d^{-1}, Table 1).

[37] In late summer and early fall surveys, the appearance of NO_3^- in surface waters, elevated *GOP* and *NCP* rates, and the TZCF were also collocated (Figure 3). However, these features were not always as tightly coupled as observed in spring. For example, during the October 2003 (CB2) cruise, the increase in productivity rates was slightly southward ($\sim$37°N) of the TZCF and NO_3^- fronts (39°–42°N); unfortunately, adverse weather prevented sampling across the entire TZCF during the 2003 cruise. During STUD08, the surface NO_3^- concentration increase, *GOP* and *NCP* rate increases, and TZCF location occurred over a narrower latitude range (40°–42°N, Figure 3). Unlike spring, the zero-crossing of northward and southward Ekman transports was substantially southward of the chemical and biological fronts, at approximately 35°N. On a regional basis, TZCF and subarctic *GOP* and *NCP* averages were comparable for summer cruises ($\approx$187–202 mmol m^{-2} d^{-1} and 27–31 mmol m^{-2} d^{-1}, for *GOP* and *NCP*, respectively). Transition and subtropical region *GOP* and *NCP* were nearly identical and about 2$\times$ lower than the TZCF/subarctic (*GOP* $\approx$ 69–80 mmol m^{-2} d^{-1} and *NCP* $\approx$ 12 mmol m^{-2} d^{-1}, Table 1).

[38] Regionally–averaged *NCP/GOP* for all cruises ranged from -0.03 to 0.23 (Figure 4 and Table 1), with summer *NCP/GOP* significantly higher than values observed in spring in all regions except for the transition region. We note that the *NCP/GOP* ratio as quantified here is analogous, but not exactly equivalent to, e-ratios and f-ratios as typically defined in the literature. To compare to historical carbon-based estimates of these "new-production" metrics, the *NCP/GOP* must be multiplied by a factor of $\approx$2 (see section 3.6). Most regional *NCP*/*GOP* averages tended to fall in the 0.05–0.20 range (Figure 4), with the low spring *NCP/GOP* in the subarctic region (0.02 $\pm$ 0.02, -0.03 ± 0.04) being the notable exception. Spatial patterns of the *NCP/GOP* ratio (Figure 3) were not identical to those tracked by the individual *NCP* or *GOP* rates. That is, in regions where *GOP* or *NCP* "peaked" the rates tended to increase proportionately to each other and the *NCP/GOP* remained constant. Highest *NCP/GOP* ratios were typically found in transition region areas where *GOP* was low and had high uncertainty (e.g., near 37°N for CB1, Figure 3 and Table S1 in Text S1).

4.2. Upper Water Column Nutrients, Pigments, Species Abundances, $^{17}\Delta_{diss}$ and $\Delta O_2/Ar$

[39] Upper water column (0–200 m) nutrient, pigment, and plankton community composition data from one spring and one summer cruise (CB1 and CB2) demonstrate similar meridional and seasonal differences to those observed in the surface data (Figure 5). Sharp gradients in N+N and chl concentrations, abundance of major picoplanktonic photoautotophs (*Prochlorococcus*, S*ynechococcus*, picoeukaryotes), and heterotrophic bacteria were observed at $\approx$33°N in spring and 37°–39°N in late summer. In both seasons, concentrations of N+N < 0.3 μmol kg^{-1} were observed in surface waters south of the TZCF, with concentrations increasing rapidly to >3 μmol kg^{-1} in surface waters north of the front. Picoplankton abundances were patchy in both seasons, but generally abundances indicated substantial shifts in community structure near the chl and N+N fronts, with *Prochlorococcus* abundant south, and heterotrophic bacteria, *Synechococcus* and picoeukaryotes abundant north of the front.

[40] Additional information on the relative rates of *GOP*, *R*, and air-sea O_2 gas exchange below the ML are supplied by the few profiles of $^{17}\Delta_{diss}$ and $\Delta O_2/Ar$ data collected during CB1 and CB2 (Figure 6). In spring, the $^{17}\Delta_{diss}$ below the ML was similar to values observed in the surface while sub-ML $\Delta O_2/Ar$ was negative. In late summer, $^{17}\Delta_{diss}$ values exceeding 100 per meg and $\Delta O_2/Ar$ of +5% to +10% were observed directly beneath the ML on isopycnals in the 23.8–25.6 range (Figure 6). These observations are consistent with a recently ventilated water column and a lack of productivity in deep, light-limited waters in spring, and the opposite (i.e., lack of ventilation, deeper euphotic zone, and significant accumulation of O_2 produced by photosynthesis in subsurface waters) over the summer period. We note that although isopycnals near the region of the TZCF indicate little resistance to deep mixing during spring, mixing would tend to bias surface $\Delta O_2/Ar$ and $^{17}\Delta_{diss}$ low during this time (more so for $\Delta O_2/Ar$, for which sub-ML values are -5%) and thus observed surface trends, which show a local maximum, are not an artifact of mixing.

Table 1. Summary of Regional Field-Based Productivity Observed on Four North Pacific Cruises[a]

	Subtropics				Transition				TZCF				Subarctic			
	CB1	P16	CB2	STUD08	CB1	P16	CB2	STUD08	CB1	P16	CB2	STUD08	CB1	P16	CB2	STUD08
Latitude Range (°N)	20–31	20–31.5	20–30	20–32	31–43	31.5–41.5	30–39	32–42	32.3–34.3	39–41	38.4–40.4	42–44	43–55	41.5–55.1	39–55	42–55
GOP	100 ± 24 (n = 4)	94 ± 16 (n = 9)	120 ± 41 (n = 3)	63 ± 7 (n = 6)	218 ± 38 (n = 9)	159 ± 27 (n = 9)	151 ± 78 (n = 4)	39 ± 11 (n = 9)	323 ± 69 (n = 3)	239 ± 49 (n = 3)	360 ± 19 (n = 2)	150 ± 41 (n = 6)	261 ± 54 (n = 5)	173 ± 24 (n = 12)	202 ± 35 (n = 6)	179 ± 26 (n = 10)
Spring	96 ± 12		–		188 ± 23		–		281 ± 38		–		199 ± 24		–	
Summer	–		80 ± 14		–		69 ± 23		–		202 ± 43		–		187 ± 20	
All	89 ± 9				134 ± 19				236 ± 31				193 ± 16			
NCP	11.2 ± 1.0	4.0 ± 2.4	10.7 ± 1.3	12.2 ± 1.5	27.8 ± 5.1	14.7 ± 1.8	22.5 ± 6.6	9.2 ± 0.7	37.9 ± 13.8	20.9 ± 1.6	40.1 ± 7.5	23.2 ± 7.8	7.8 ± 4.2	0.8 ± 3.9	18.2 ± 8.0	38.0 ± 6.2
Spring	6.0 ± 1.9		–		21.2 ± 3.0		–		29.4 ± 6.6		–		2.8 ± 3.0		–	
Summer	–		11.5 ± 0.9		–		12.7 ± 2.2		–		27.4 ± 6.1		–		30.6 ± 5.2	
All	8.3 ± 1.3				17.4 ± 2.1				28.3 ± 4.5				16.3 ± 3.8			
NCP/GOP	0.13 ± 0.02	0.05 ± 0.02	0.10 ± 0.02	0.20 ± 0.02	0.15 ± 0.03	0.10 ± 0.01	0.17 ± 0.07	0.19 ± 0.02	0.12 ± 0.03	0.09 ± 0.01	0.11 ± 0.03	0.15 ± 0.02	0.02 ± 0.02	−0.03 ± 0.04	0.07 ± 0.03	0.23 ± 0.04
Spring	0.07 ± 0.02		–		0.13 ± 0.02		–		0.10 ± 0.01		–		−0.01 ± 0.03		–	
Summer	–		0.17 ± 0.02		–		0.14 ± 0.03		–		0.14 ± 0.02		–		0.17 ± 0.03	
All	0.11 ± 0.02				0.13 ± 0.02				0.13 ± 0.01				0.08 ± 0.03			

[a]Latitude range for regions determined based on position of the subtropical and subarctic front as defined by *Roden* [1991] (see text). *GOP* (mmol O_2 m^{-2} d^{-1}), *NCP* (mmol O_2 m^{-2} d^{-1}), and *NCP*/*GOP* (unitless) are given as the mean value ± standard error of the mean. Number of observations in each region is also given. Observations where *GOP* = 0 or the *GOP* is not significantly different than zero have been excluded from the *NCP*/*GOP* average. Individual *NCP*, *GOP*, and *NCP*/*GOP* are given in the auxiliary material (Table S1 in Text S1).

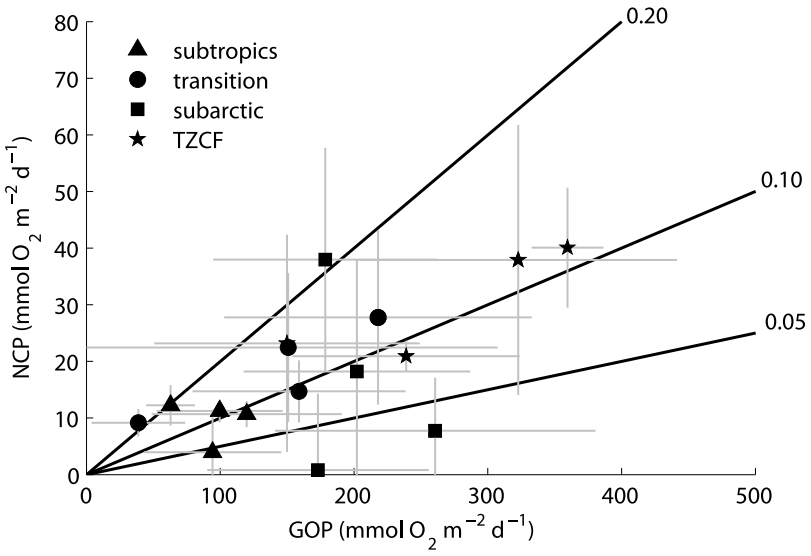

Figure 4. Regional average *NCP* and *GOP* for each cruise, with x- and y-error bars (thin gray lines) depicting the standard deviation for each region. Values are given in Table 1. Also shown for reference are lines of constant *NCP/GOP* (solid black lines).

[41] We can use the spring/fall snapshots provided by the April (CB1) and October (CB2) 2003 cruise data to calculate a rough estimate of biological production below the ML in seasonal thermocline waters (50–150 m) in the transition region. If treated as a closed system, the $^{17}\Delta_{diss}$ inventory change $\left(\frac{d[O_2]^{17}\Delta}{dt}\right)$ accumulated over ~180 days between observations (or, to be more exact, the $\delta^{17}O$ and $\delta^{18}O$ inventory change [cf. *Kaiser*, 2011, equation 42]) implies a gross photosynthetic O_2 input ranging from approximately 1 to 3 mmol m^{-3} d^{-1} near the base of the ML to zero at depths of 100–150 m. At 32°N and 40°N the column-integrated *GOP* is similar, ≈50 mmol m^{-2} d^{-1}, although the production is distributed over the entire 50–150 m interval at 32°N, and only over 50–100 m at 40°N. Changes in total O_2 inventory over the 180 day period also constrain a rough estimate of *NCP* in the seasonal thermocline. Over the 50–150 m interval there was a slight (32°N) or substantial decrease (40°N) in total O_2 inventory, likely because any net O_2 accumulation near the base of the ML due to *NCP* was compensated for by enhanced consumption at 75–150 m. If integrated over a shallower depth horizon (50–75 m), the $\frac{d[O_2]}{dt}$ at 40°N is still negative (−1.5 mmol m^{-2} d^{-1}), but at 32°N is positive, 1.3 mmol m^{-2} d^{-1}, ≈10% of summer *NCP* in the subtropical and transition region ML. Because these simple calculations neglect diapycnal transport of accumulated $^{17}\Delta_{diss}$ and O_2 into waters above/below the given depth intervals, they are likely minimum estimates.

4.3. Comparison to Historical GOP, NPP, and NCP Rates at HOT and OSP

[42] Although the seasonal distribution of *GOP* and *NCP* in this study is limited, our meridional surveys of the NE Pacific subtropical, transition, and subarctic regions provide a unique opportunity to evaluate biological productivity rates measured at HOT and OSP in a broader, regional context (Figure 7). In general, subtropical region *GOP* in this study was within reported uncertainty of seasonally averaged $^{17}\Delta$–based *GOP* observed at HOT during 2006–2008 (gray boxes, Figure 7a [*Quay et al.*, 2010]) as well as $^{17}\Delta$–based *GOP* determined on four ship-of-opportunity crossings of the eastern subtropical gyre region (white circles, Figure 7a [*Juranek and Quay*, 2010]). Results are also in good agreement with the seasonal average ^{14}C-based productivity from HOT compiled by *Brix et al.* [2006] (black bars, Figure 7a) if a *GOP/NPP* ratio of 2.7 is assumed (see section 3.6 but note, however, that HOT uses 12hr -^{14}C incubations and thus the GOP/^{14}C-incubation ratio is likely to be less than 2.7 because of reduced recycling of ^{14}C labeled organic carbon over a shorter duration experiment). Subtropical region *NCP* in this study was also close to summer/winter season averages determined from $\Delta O_2/Ar$ at HOT (gray bars, Figure 7b [*Quay et al.*, 2010]) and seasonal DIC-based *NCP* from HOT (black bars, Figure 7b [*Brix et al.*, 2006]). The overall average subtropical region *NCP* from the two spring, two summer cruises in this study, 8.3 ± 1.3 mmol m^{-2} d^{-1}, was also in very good agreement with the mean of several annual O_2 and C–based budgets at HOT (10.1 mmol (O_2) m^{-2} d^{-1}, solid black line, Figure 7b; see Table 2 for references and individual values). The overall agreement between our seasonally–limited *NCP* and *GOP* and longer-term historical averages at HOT is likely due to the relatively weak seasonality in the subtropical region.

[43] There are no previous estimates of *GOP* from the NE subarctic Pacific, but there is an abundant historical database of primary productivity determined by ^{14}C-incubations. If converted to a NPP-equivalent rate (section 3.6), subarctic region $^{17}\Delta$–based *GOP* was significantly higher than previously measured ^{14}C-NPP at OSP during spring, while in late summer the GOP and historical ^{14}C-NPP are in reasonable agreement (black bars, Figure 7c [*Wong et al.*, 1995; *Boyd and Harrison*, 1999; *Welschmeyer et al.*, 1993; *Harrison*, 2002]). The discrepancy in observed rates for spring could indicate one of several things: (1) the ratio of

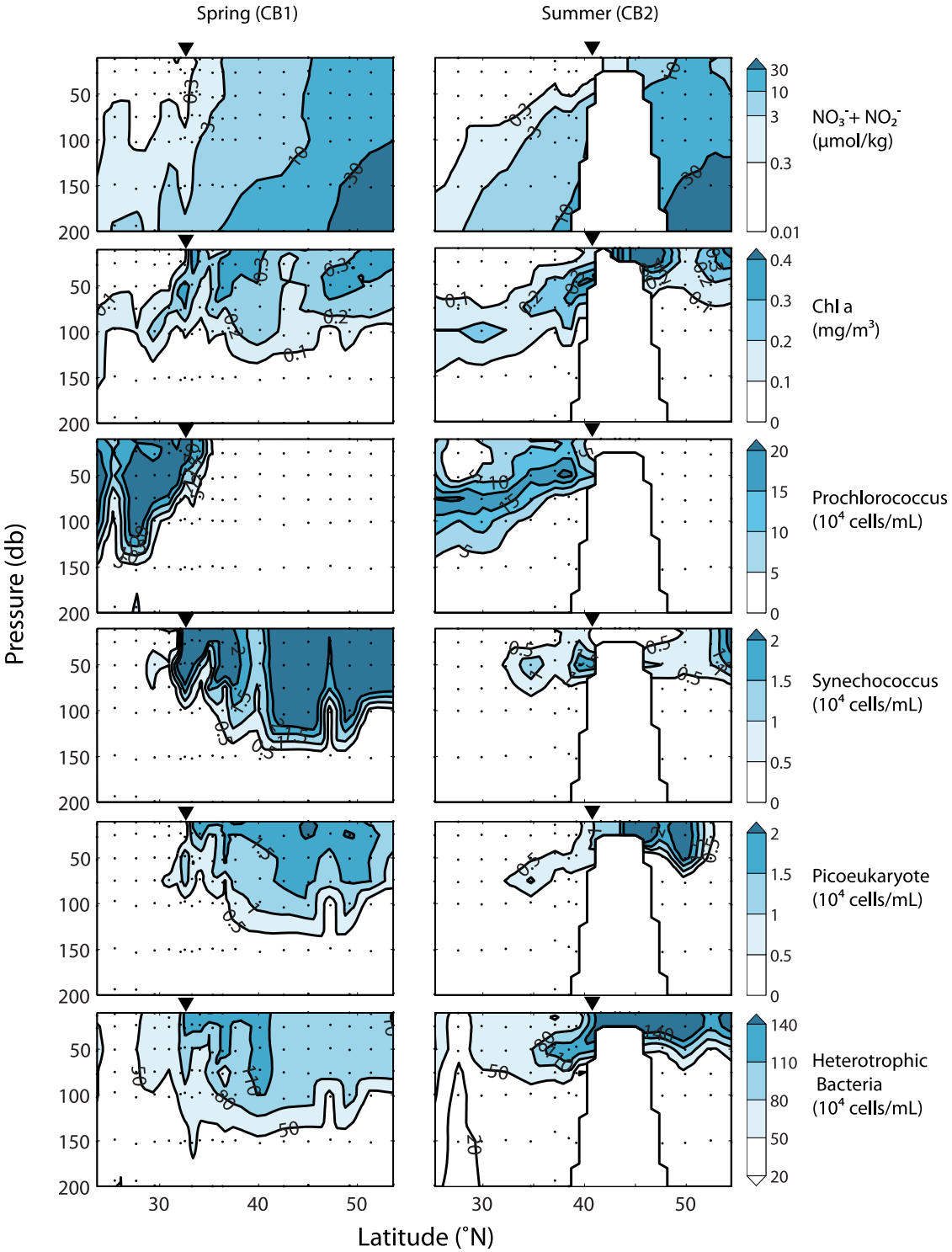

Figure 5. Upper water column trends observed on the spring and late-summer CB1 and CB2 cruises. Shown are N+N, chl a, and abundances of *Prochlorococcus*, *Synechoccocus*, Picoeukaryotes, and Heterotrophic Bacteria determined by flow cytometry. Inverted triangle at the top of each figure indicates approximate TZCF location for each cruise.

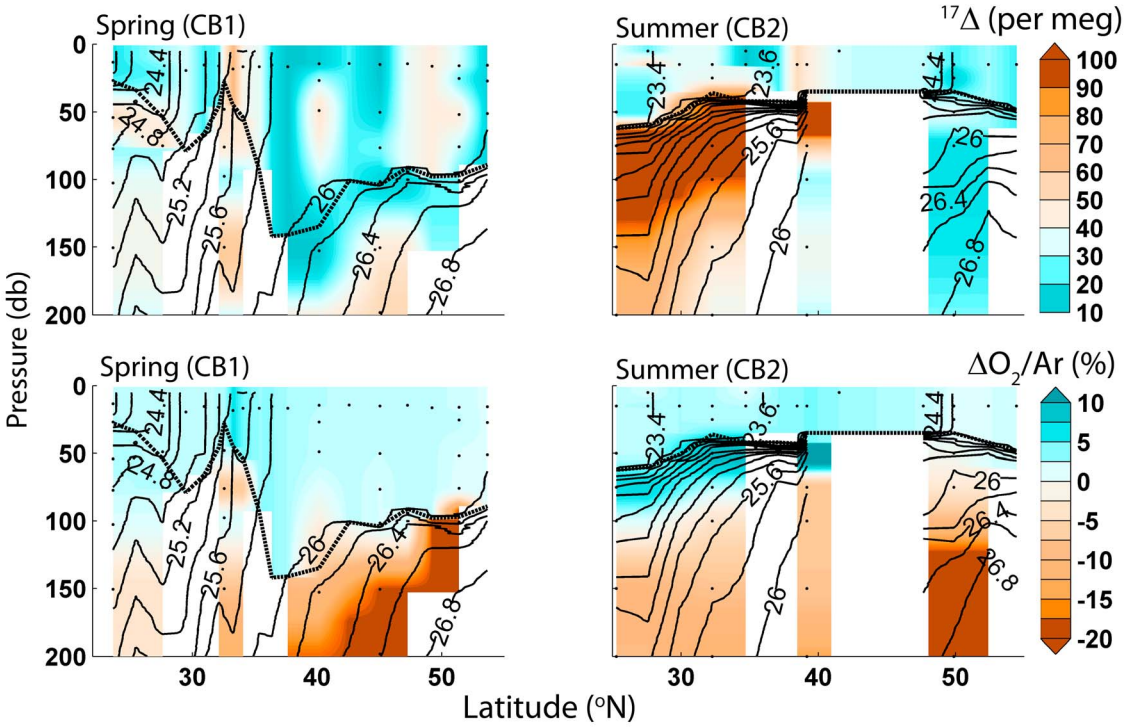

Figure 6. Sections of dissolved gas tracers $^{17}\Delta_{diss}$ and $\Delta O_2/Ar$ observed on spring and summer cruises in 2003 ((left) CB1 and (right) CB2). Overlaid are density contours (thin black lines) increasing at 0.2 kg m^{-3} intervals as well as the calculated ML depth (thicker black line) determined as the depth where σ_θ is 0.125 kg m^{-3} greater than the surface [*Monterey and Levitus*, 1997]. Profiles collected during the other spring cruise (P16N) display similar trends and are not shown here. Profiles collected for STUD08 (28°N, 44°N, 46°N) were too sparse to permit contouring.

GOP/^{14}C-PP is greater than 2.7 at this time of year (see section 3.6); (2) *GOP* (and *NPP*) rates are higher in early spring (March–April), but this timeframe has not been historically well-sampled by seasonal cruises at OSP which are typically in February, June, and August; (3) our observations coincided with two anomalous spring productivity "events;" or (4) the difference in integration timescales between the incubation and O_2–budget approach cause real differences in measured rates. Without coincident observations of ^{14}C–PP and $^{17}\Delta$–*GOP* [e.g., *Quay et al.*, 2010] it is impossible to determine which of the above is responsible.

[44] The comparison of subarctic region *NCP* to previous estimates (Figure 7d) is complicated by temperate seasonality and potential mixing biases. Spring *NCP* in this study was very low (1–8 mmol m^{-2} d^{-1}) compared to late summer observations (18–38 mmol m^{-2} d^{-1}). However, given typical residence times for O_2 of 20 days ($z_{ML} \approx 100$ m, $k_{O2} \approx 5$ m d^{-1}), the spring *NCP* estimates could certainly be influenced by winter mixing events which would bring low $\Delta O_2/Ar$ water from depth to the surface. Thus, we would consider spring *NCP* minimum estimates. K. Giesbrecht et al. (Biological productivity along Line P in the subarctic northeast Pacific: In-situ versus incubation-based methods, submitted to *Global Biogeochemical Cycles*, 2012) recently reported $\Delta O_2/Ar$–based *NCP* at OSP for February, June, and August cruises throughout 2007–2009 (Figure 7d, gray bars show 3 year averages, open circles denote anomalous single-cruise results). Because of winter season mixing biases, in only one of the three years was February *NCP* positive (open circle, Figure 7d); otherwise measured $\Delta O_2/Ar$ were negative. Summer averages reported by Giesbrecht et al. (submitted manuscript, 2012) (gray bars, Figure 7d) were close to the CB2 October average. In addition, the high *NCP* determined by Giesbrecht et al. (submitted manuscript, 2012) in August 2008 (white circle, Figure 7d), one month before our September 2008 observations, is very close to our own estimate. Both the August 2008 Giesbrecht et al. (submitted manuscript, 2012) *NCP* and our September 2008 STUD08 *NCP* were observed following a natural iron fertilization event from volcanic ash deposition (as described in *Hamme et al.* [2010]) and thus may be atypically high. The mean of several summer-season budgets of O_2 (or ΔNO_3^-) reported in Table 2 is 2.1 mol C yr^{-1}, corresponding to an average daily rate of 16 mmol O_2 m^{-2} d^{-1} if a 6 month summer growing season is assumed (these budgets assume *NCP* < 0 in winter). The mean subarctic *NCP* for the summer cruises in this study was considerably higher (30.6 ± 5.2 mmol m^{-2} d^{-1}, Table 1), but if the potentially anomalous STUD08 cruise results are omitted (leaving just the CB2 results), the summer subarctic average is similar (18.2 ± 8.0 mmol m^{-2} d^{-1}, Table 1).

[45] The transition region has been studied using hydrography, space-borne observations, and ecosystem models [*Roden*, 1980, 1991; *Glover et al.*, 1994; *Polovina et al.*, 2001, 2008; *Chai et al.*, 2003], but few prior field-based biological rate measurements exist in this region. *Howard et al.* [2010]

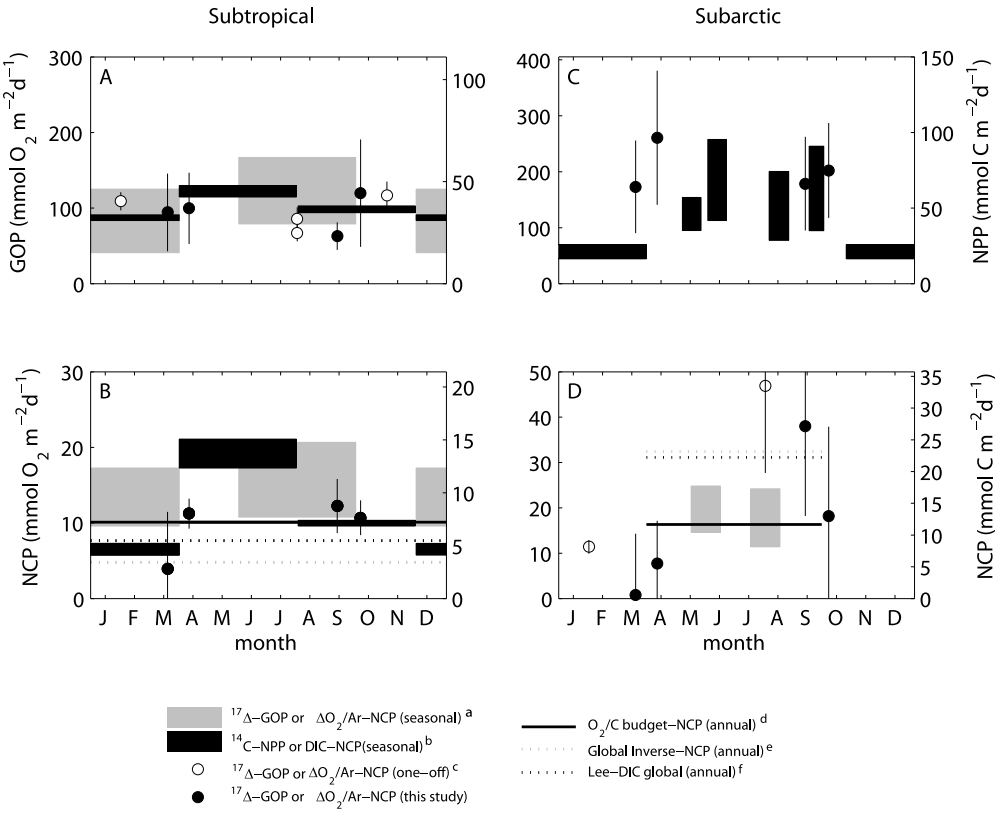

Figure 7. Comparison of *GOP* and *NCP* observed in this study to previous historical estimates. Bar widths denote month(s) of observations and height denotes reported variability of observations (e.g., mean ± standard deviation). Dual y-axes on top and bottom plots are scaled so that *GOP* = 2.7NPP and *NCP*(O_2) = 1.4*NCP*(C) (see section 3.6). Note that subtropical and subarctic figures have different scaling for readability, and that some error bars are offscale. References for literature values are as follows: a, subtropical $^{17}\Delta$–*GOP* and $\Delta O_2/Ar$–*NCP*: *Quay et al.* [2010], subarctic $\Delta O_2/Ar$–*NCP*: Giesbrecht et al. (submitted manuscript, 2012); b, subtropical ^{14}C-NPP and DIC-*NCP*: *Brix et al.* [2006], subarctic ^{14}C-NPP: *Welschmeyer et al.* [1993], *Boyd et al.* [1995], and *Boyd and Harrison* [1999]; c, subtropical $^{17}\Delta$–*GOP*: *Juranek and Quay* [2010], subarctic $\Delta O_2/Ar$-NCP: Giesbrecht et al. (submitted manuscript, 2012); d, subtropical: average of annual timescale NCP estimates based on O_2, DIC and ^{234}Th budgets summarized by *Emerson et al.* [2008] and reported in Table 2, subarctic: average of NCP estimates derived from seasonal NO_3^- drawdown, ^{234}Th, and O_2 mass balances summarized by *Emerson and Stump* [2010] and reported in Table 2; e, basin-scale inversion of O_2, nutrients, and carbon [*Schlitzer*, 2004]; f, NCP derived from seasonal DIC drawdown predicted from empirical algorithms and pCO_2 climatology [*Lee*, 2001].

recently reported a mean *NCP* of 4.8 mmol m^{-2} d^{-1} for two cruises in the region, including the September 2008 (STUD08) cruise. Their STUD08 *NCP* rates, determined from three stations in the transition region using $\Delta O_2/Ar$ determined from an ^{36}Ar isotope dilution technique (on independent samples), was roughly half of the mean for the nine stations in this study. The reason for the discrepancy is unclear, but equilibrated seawater standards run periodically with our samples are typically within ± 0.1% of the expected O_2/Ar value, and the good agreement between our subtropical/subarctic region results and other data at HOT and OSP indicate that that the *NCP* estimates in all regions are robust. D. Lockwood et al. (High-resolution estimates of net community production and air-sea CO_2 flux in the Northeast Pacific, submitted to *Global Biogeochemical Cycles*, 2012) also determined transition region *NCP* on the STUD08 cruise from continuous underway $\Delta O_2/Ar$ measured by equilibrator inlet mass spectrometer. Their reported average for 32°–40°N, based on thousands of individual $\Delta O_2/Ar$ determinations, was 5.9 ± 2.5 mmol C m^{-2} d^{-1}, very close to the value determined from the more limited data set in this study (6.6 mmol C m^{-2} d^{-1}).

[46] The reasonable agreement between *GOP* and *NCP* rates observed in this study and previous estimates at HOT and OSP is of particular interest, because it suggests that time series observations are likely to be representative of mean productivity rates at the regional-scale. This is an encouraging result, since the historical lack of biological rate observations outside of the time series sites creates some uncertainty when these geographically limited data are scaled up to regional estimates. However, our observations also indicate that the transition region, and specifically, the TZCF, functions uniquely, unlike adjacent subtropical and subarctic regions in both a hydrographic and biological sense. Thus, some caution should be exercised in basin-scale

Table 2. Annual Air-Sea CO_2 Flux and Biologically Induced CO_2 Flux Along 152°W

Observed/Modeled CO_2 Flux Component	Subtropical (20°N–32°N)	Transition (32°N–42°N)	Subarctic (42°N–55°N)
Total air-sea CO_2 flux[a]	0.8	0.8–2.0	1.5–2.0
Biological CO_2 flux			
NCP: this study[b]	2.2	3.4	2.1
NCP: prior estimates from O_2, DIC, NO_3^-, and ^{234}Th budgets	2.7,[c] 1.4,[d] 4.3,[e] 2.4,[f] 2.7,[g] 2.3[h]	(0.9),[i] (2.1)[j]	2.5,[k] 1.8,[l] 2.1,[m] 1.6,[n] 2.5[o]
NCP-climatology, inversion based estimates	1.3,[p] 2,[q] 2.5[r]	2.5,[p] 3,[q] 3[r]	4.2,[p] 4.0,[q] 1.5[r]
NCP-CO_2 model[s]	1.4	1.5–2.8	2.0

[a] *Takahashi et al.* [2009]. Values taken from climatological boxes along 152°W.
[b] Annual fluxes computed from average of all four cruises, assuming average daily rates over growing season of 12 months (subtropical), 9 months (transition), and 6 months (subarctic).
[c] *Emerson et al.* [1997].
[d] *Hamme and Emerson* [2006].
[e] *Emerson et al.* [2008].
[f] *Benitez-Nelson et al.* [2001].
[g] *Quay and Stutsman* [2003].
[h] *Keeling et al.* [2004].
[i] *Howard et al.* [2010]. Parentheses indicate annual value scaled up from two-cruise average and is thus not well constrained.
[j] Lockwood et al. (submitted manuscript, 2012). Parentheses indicate annual value scaled up from single cruise and is thus not well constrained.
[k] *Wong et al.* [2002].
[l] *Charette et al.* [1999].
[m] *Emerson* [1987].
[n] *Emerson et al.* [1991].
[o] *Emerson and Stump* [2010].
[p] *Schlitzer* [2004].
[q] *Lee* [2001].
[r] Sonnerup et al. (manuscript in preparation, 2012).
[s] Rough estimate of *NCP* from modeled CO_2 budget, assuming negligible impact of transport processes on carbon mass balance during summer months (see section 6 for details).

extrapolations. Estimates of primary production or organic carbon export produced from remote sensing observations and calibrated/validated with time series rate data [*Behrenfeld and Falkowski*, 1997; *Westberry et al.*, 2008; *Laws et al.*, 2000], in particular, may need to be carefully evaluated in this region [*Juranek*, 2007].

4.4. Comparison to Estimates of NCP From Basin-Scale Inversions and Models

[47] Caveats regarding differences in integration timescales need to be taken into account when comparing short-term, regionally–averaged *NCP* from this study to estimates derived from models and climatological tracer fields which integrate over annual to decadal timescales. For example, in the subtropical N. Pacific, the mean *NCP* for this study, 8.3 ± 1.3 mmol O_2 m^{-2} d^{-1} (5.9 ± 0.9 mmol C m^{-2} d^{-1}) was nearly identical to *NCP* derived from climatology-estimated seasonal surface DIC drawdown (5.5 mmol C m^{-2} d^{-1}, Figure 7b [*Lee*, 2001]) but a factor of 2 higher than the average daily rate predicted by an inversion of O_2, nutrient, and carbon fields (3.4 mmol C m^{-2} d^{-1} for annual export of 1.3 mol C m^{-2} divided by 365 days [*Schlitzer*, 2004], Table 2). It is tempting to resolve this discrepancy by suggesting that surface-derived *NCP* in the subtropics is higher than the exported flux remineralized at depth, i.e., a substantial fraction of organic carbon production is remineralized in the seasonal thermocline which re-equilibrates with the atmosphere in winter. However, a recent estimate of *NCP* derived from AOU observed in the permanent thermocline (200–500 m) and an improved age model constrained by CFC and SF_6 measurements (i.e., less biased by diapycnal mixing) is comparable to our subtropical estimate (annual export of 2.5 mol C m^{-2}, for mean daily rate of 6.8 mmol C m^{-2} d^{-1} (R. S. Sonnerup et al., Transit time distributions and oxygen utilization in the Northeast Pacific Ocean from chlorofluorocarbon and sulfur hexafluoride, manuscript in preparation, 2012), Table 2).

[48] The summer subarctic average *NCP* in this study, 30.6 ± 5.2 mmol O_2 m^{-2} d^{-1} (21.9 ± 3.7 mmol C m^{-2} d^{-1}), was nearly identical to the value calculated from the *Lee* [2001] and *Schlitzer* [2004] *NCP* estimates if a 6 month growing season is assumed (e.g., annual export of 4 mol C m^{-2} yr^{-1} and 50 g C m^{-2} yr^{-1}, respectively, yields ≈20–25 mmol C m^{-2} d^{-1} for 6 month growing season, Figure 7d and Table 2). However, as noted above, the subarctic summer average was potentially biased high by an anomalous fertilization event [*Hamme et al.*, 2010]. The mean for the summer cruise not influenced by this event, CB2, was 13 mmol C m^{-2} d^{-1}, much lower than the *Lee* and *Schlitzer* estimates for this region, but closer to the regional estimate constrained by AOU and CFC/SF6 age (annual export of 1.5 mol C m^{-2}, for daily average of 8.3 mmol C m^{-2} d^{-1} over 6 months; Table 2) (Sonnerup et al., manuscript in preparation, 2012).

[49] Because the seasonality of *NCP* in the transition region is not well-characterized, it is difficult to compare *NCP* derived from longer-term integrations with those in our study. Mean *NCP* in this study, 17.4 ± 2.1 mmol O_2 m^{-2} d^{-1} (12.4 ± 1.5 mmol C m^{-2} d^{-1}) was 1.5–2× higher than the average daily rate calculated from the *Lee* [2001], *Schlitzer* [2004], and Sonnerup et al. (manuscript in preparation, 2012) estimates if annual *NCP* is assumed to be evenly distributed across 12 months (i.e., annual NCP of 2.5–3 mol C m^{-2} yr^{-1}, daily rate of 6–8 mmol m^{-2} d^{-1}; Table 2). A growing season (i.e., $NCP > 0$) of 9 months, intermediate between the subtropics, which has $NCP > 0$ for 12 months [*Quay et al.*, 2010], and the subarctic, which has $NCP > 0$ for ≈6 months [*Emerson et al.*, 1991] would bring the daily

rate measured in this study into reasonable agreement with the others (annual export of 3.4 mol C m^{-2}, Table 2). Thus, the transition region, which has short-term rates that are comparable to those observed in the subarctic, but a potentially longer-term growing season, offers regional potential for enhanced biologically regulated CO_2 uptake.

5. Controls on North Pacific Productivity Near the TZCF

[50] The substantial differences in *GOP* and *NCP* rates, pigments, and plankton community structure observed at the NO_3^- front and TZCF suggest that fundamental changes in biological carbon cycling occur at this boundary. The location of the front(s) relative to the meridional Ekman transport (v_{Ek}) convergence for our two spring and two summer cruises in the NE Pacific appear to be consistent with the *Ayers and Lozier* [2010] hypothesis regarding the physical control of seasonal TZCF migration (see section 2, Figure 3). Our results further augment the *Ayers and Lozier* [2010] hypothesis by indicating that the TZCF is associated with elevated *GOP* and *NCP* relative to adjacent regions north and south of the front. These observations raise a few interesting questions: What processes are responsible for increased *GOP* and *NCP* at the front? Are the mechanisms controlling productivity at the TZCF as it migrates through the region in summer similar to those observed in early spring and late summer when the TZCF is at its most northern/southern extreme? The second question is difficult to answer in the absence of mid-summer data near the TZCF, but an answer to the first question, i.e., an understanding of the mechanisms controlling *GOP* and *NCP* near the TZCF in early spring and late summer, may offer some insight.

[51] To understand mechanisms for enhanced production, examination of plankton community composition is essential. With regards to picophytoplankton, the TZCF appears to delineate a boundary between a subtropical autotrophic community dominated by *Prochlorcoccus* and a subarctic community composed of *Synechococcus* and picoeukaryotes (Figure 5). The availability of different nitrogen sources could explain some of this ecological partitioning, as numerous strains of *Synechococcus* and picoeukaryotes can utilize NO_3^- directly while the dominant strains of *Prochlorococcus* lack nitrate reductase [*Rocap et al.*, 2003]. *Church et al.* [2008] also identified active N_2-fixation gene transcription for several groups of cyanobacteria south (but not north) of the TZCF/NO_3^- front during CB1 and CB2. Thus, the movement of the TZCF and NO_3^- front could also be viewed as an expansion/contraction of the planktonic ecotypes associated with the subtropical/subarctic gyre. But why would meridional transport of NO_3^- stimulate productivity at the front in spring (as suggested by *Ayers and Lozier*, [2010])? The delivery of NO_3^- would presumably not stimulate the productivity of *Prochlorococcus*, which mostly lack the capacity to utilize NO_3^-, and subarctic photoautotrophs north of the TZCF (*Synechococcus* and picoeukaryotes) are likely not N-limited as concentrations of NO_3^- in the high-nutrient low-chlorophyll subarctic gyre rarely approach zero [e.g., *Harrison*, 2002].

[52] The hydrography in the region of the TZCF (Figure 2) may provide some clues. During the April 2003 (CB1) cruise, isopycnals were near–vertical from the surface to 200 m depth (Figure 2). Thus, an enhanced delivery of limiting nutrients from depth might be expected. Delivery of dissolved iron from depth could support a bloom of eukaryotic photoautotrophs (e.g., diatoms) in micronutrient-limited surface waters of the high-nitrate low-chl subarctic gyre [*Boyd and Harrison*, 1999; *Whitney et al.*, 2005; *Lam et al.*, 2006], and Fe and P–"excess" (NO_3^-: PO_4^{3-} < 16) could stimulate a bloom of N_2-fixing diazotrophs in the low nitrate, low chl subtropical gyre [*Karl and Letelier*, 2008] or coccolithophores in the subarctic [*Painter et al.*, 2010]. Recently, deep water injections of nutrients have been linked to periods of higher than usual O_2 saturation (i.e., *NCP* "events") observed from profiling Argo floats in the subtropical region near HOT [*Johnson et al.*, 2010]. Similarly, results of a 1-D upper ocean model at OSP indicate periodic supply of iron from depth is required to maintain observed biological production [*Steiner et al.*, 2007]. Of course, light would still be a limiting factor for phytoplankton growth, but we note that the ML depth (determined using a 0.125 σ_θ density criterion) also shoals rapidly from 100 m to 50 m in the vicinity of the TZCF during the CB1 cruise (Figure 6). Thus, in the vicinity of the TZCF the ML likely provides adequate light for diatom, diazotroph, or coccolithophore growth.

[53] Pigment and satellite data support the hypothesis that eukaryotic phytoplankton activity is stimulated near the TZCF. HPLC pigment data from the spring 2003 cruise (CB1) display a local maximum in fucoxanthin (a diatom indicator), and 19′-Hexanoyloxyfucoxanthin (19′-Hex, a prymnesiophyte biomarker) at the TZCF (http://hahana.soest.hawaii.edu/cookbook/). Satellite-based estimates of particulate inorganic carbon (PIC) for the timeframe prior to and coincident with the CB1 cruise (30 March to 14 April 2003) also display a marked increase at 33°N (Figure 8). During the late- summer CB2 cruise, HPLC pigments display an approximate doubling in 19′-Hex near the TZCF between 35°–40°N with only slight increases in fucoxanthin, while MODIS-based PIC indicates a doubling between 38°–42°N (Figure 8). A strongly–stratified water column, as observed during this cruise (Figure 2), would prevent delivery of micronutrients from depth and tend to favor coccolithophores (a marine prymensiophyte that creates a $CaCO_3$ exoskeleton) over diatoms [*Painter et al.*, 2010]. No HPLC pigment data are available for the other two cruises, but MODIS-Aqua PIC concentrations show similar increases at the TZCF, with September 2008 (STUD08) cruise PIC sevenfold higher than south of the front.

[54] From these satellite and field based observations, it seems likely that the elevated *GOP* and *NCP* observed at the TZCF is at least partially supported by coccolithophore production. Diatoms may also contribute when the TZCF coincides with the enhanced delivery of micronutrients from depth to the surface, as seen for CB1 (Figure 2). Relative supply rates of iron from depth (dependent on the degree of water column stratification) may explain the different trends in *GOP* and *NCP* observed in the region of the TZCF for individual cruises. For example, the more moderate *GOP* and *NCP* observed near the TZCF during P16N may be explained by the atypical hydrographic conditions observed for this cruise relative to the other spring cruise (Figure 2), with warmer, less dense water preventing deep-mixing in the region of the TZCF (35°–37°N). The extremely high PIC observed during STUD08, which followed the August 2008 natural iron fertilization event stimulated by volcanic ash

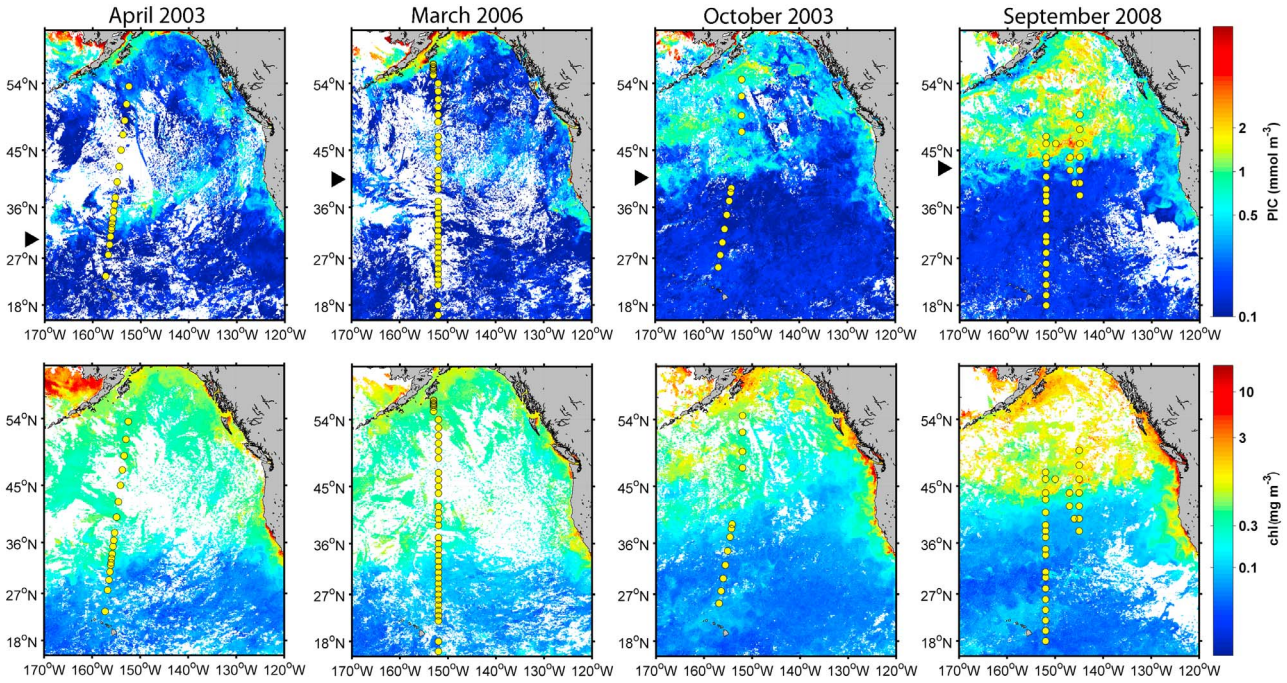

Figure 8. (top) Estimates of particulate inorganic carbon concentration (mmol m^{-3}) from MODIS-Aqua [*Balch et al.*, 2005], with the approximate position of the TZCF intersection with the cruise track indicated with solid black arrow on the left of each figure. (bottom) SeaWiFS chl a for 2 week periods prior to and concurrent with the four cruises.

deposition [*Hamme et al.*, 2010], may have been a secondary coccolithophore bloom following the decline of an initial diatom bloom. Diatoms are expected to be favored under iron-replete conditions, while coccolithophores would be favored under stratified, but iron-deplete, conditions [*Painter et al.*, 2010].

[55] An important question to consider is whether or not elevated *GOP* and *NCP* rates observed at the front represent an isolated event, rather than steady state conditions (and thus rates determined using a steady state assumption inaccurate). While the data limitations imposed by snapshot surveys require this steady state assumption (i.e., we have no information on the time-variability in $^{17}\Delta_{diss}$ and $\Delta O_2/Ar$), several arguments indicate the *GOP* and *NCP* rates at the TZCF are not biased high as a result of nonsteady state processes. First, the appearance of elevated $^{17}\Delta_{diss}$ and $\Delta O_2/Ar$ at the front on four separate occasions is an indication that enhanced productivity is a persistent, rather than ephemeral, feature. Second, the observation that *NCP* and *GOP* increase proportionately, and the *NCP/GOP* ratio remains relatively constant across the TZCF (Figure 3) indicates these rate terms are tightly coupled, and not decoupled (i.e., higher NCP/GOP or e-ratio) as might be expected under a bloom or event [e.g., *Luz et al.*, 2002; *Denman et al.*, 2006]. Regardless, the $^{17}\Delta_{diss}$ and $\Delta O_2/Ar$ values observed in the vicinity of the TZCF, 60–70 per meg, +3–6%, respectively (e.g., see Figure 6), are independent tracers of intense biological activity. If not at steady state, it would still require a substantial increase in *GOP* and *NCP* to achieve observed $^{17}\Delta_{diss}$ and $\Delta O_2/Ar$ values within the 10–15 day timescale over which the tracers integrate (a function of the residence time with respect to air-sea O_2 gas exchange). For example, with a k_{O2} = 5 m d^{-1} and z_{ML} = 50 m, a rate at least 5× background would be needed to raise $^{17}\Delta_{diss}$ from 35 per meg to the 60–70 per meg range over a 15 day period. This is largely because air-sea O_2 gas exchange removes the photosynthetically produced, high–$^{17}\Delta_{diss}$ O_2 continually. Thus, whether conditions are at steady state or not, tracer data indicate enhanced *GOP* and *NCP* in the vicinity of the TZCF.

[56] Taken as a whole, these data suggest that *GOP* and *NCP* near the TZCF are elevated, and that vertical micronutrient supply, stratification, and taxa shifts (from prokaryotes to diatoms and coccolithophores) may provide potential mechanisms for the enhanced productivity. In the spring, the TZCF productivity may be supported by a combination of diatom and coccolithophore production, depending on isopycnal slopes, while under stratified summer conditions, it seems likely that coccolithophore production would be favored (in the absence of external iron inputs). If *NCP* is similarly elevated at the TZCF throughout the summer, the TZCF would support an enhanced *NCP* (and potential export flux) on the order of 15% above background. That is, if "additional" *NCP* near the TZCF (Figure 3) has an area approximated by 1/2(base)(height), ≈1/2(50 mmol m^{-2} d^{-1})(2°), and background *NCP* is ≈(12 mmol m^{-2} d^{-1})(30°), the ratio of enhanced /background *NCP* is = 0.14. Thus, enhanced productivity at the TZCF may play an important regulatory role in the annual cycle of air-sea CO_2 exchange in this globally–important N. Pacific CO_2 sink region.

6. Biologically Induced Air-Sea CO_2 Fluxes

6.1. Comparisons of NCP to Observed Net Air-Sea CO_2 Flux and Climatology

[57] The impact of the biological pump on net air-sea CO_2 flux in the N. Pacific sink region has been discussed

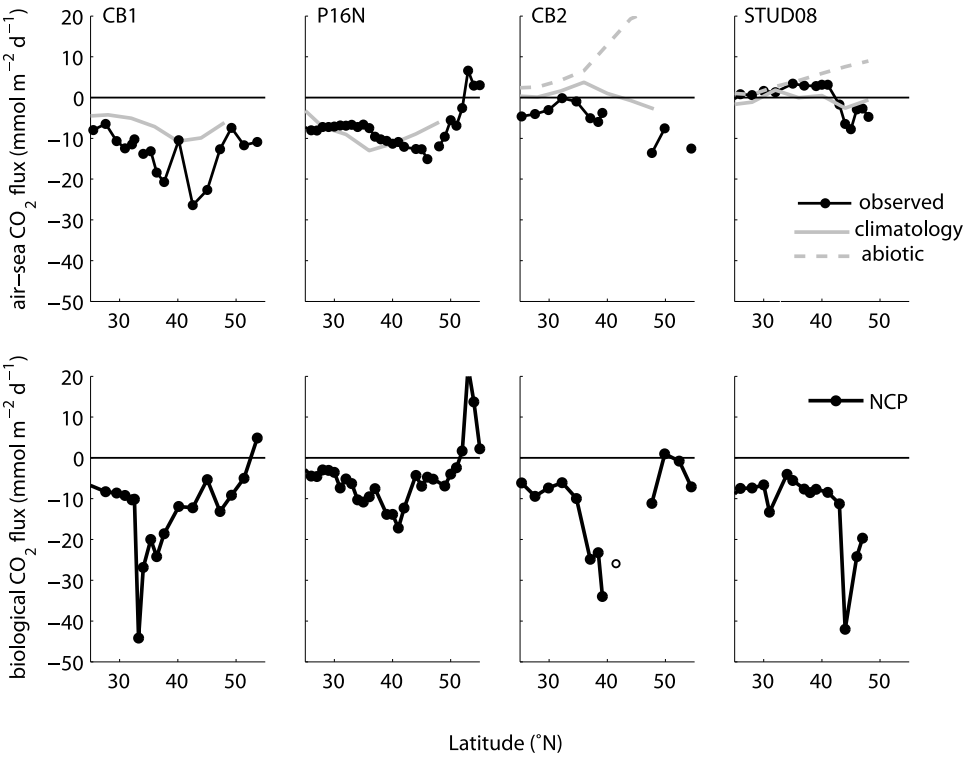

Figure 9. Air-sea CO_2 flux and biological CO_2 flux (*NCP*) observed on the four N. Pacific surveys. (top) Observed and climatological CO_2 flux; summer cruises also show an "abiotic" gas flux which is calculated from early spring $pCO_{2,w}$ and the late summer temperature (i.e., only gas solubility affects $pCO_{2,w}$). (bottom) *NCP*, converted to a carbon equivalent using a photosynthetic quotient ($\Delta O_2/\Delta CO_2$) of 1.4 for new production [*Laws*, 1991].

previously [e.g., *Takahashi et al.*, 2002, 2009; *Chierici et al.*, 2006], but never in the context of concurrent biological rate terms *GOP* and *NCP. Takahashi et al.* [2002] evaluated the annual cycle of air-sea CO_2 flux near OSP from a global pCO_2 climatology and determined that a biological CO_2 drawdown of 115 μatm was needed to counteract the expected 105 μatm increase from decreasing solubility (increasing SST) during the summer. Thus, in the absence of biological activity the region would be a moderate source of CO_2 to the atmosphere during summer, but instead the region is neutral or a weak sink.

[58] On an annual basis, it is clear that both the biological and solubility pumps are important determinants of the net CO_2 flux, but many previous studies have lacked an explicit accounting of the physical transport of CO_2 outside of the study area (i.e., the "pump" of the solubility pump) leading to ambiguity regarding the relative strength of each. Recently, *Ayers and Lozier* [2012] evaluated terms controlling surface ocean pCO_2 on a monthly basis throughout the N. Pacific basin, with a focus on the transition zone where the net annual CO_2 flux is greatest. Their analysis revealed that while solubility and biological productivity (the latter modeled using satellite algorithms and various e-ratio formulations) were dominant terms controlling air-sea CO_2 flux on a seasonal scale, biological productivity and geostrophic transport of DIC were the two most important terms determining uptake on an annual basis. The spatial relation of geostrophic DIC transport and annual air-sea CO_2 flux (and the lack of spatial relation in the biological CO_2 flux) led the authors to conclude that advection of DIC determines the location of the CO_2 sink on an annual basis. However, the satellite productivity algorithms used in their study [*Behrenfeld and Falkowski*, 1997; *Westberry et al.*, 2008] do not replicate the meridional trends observed here [*Juranek*, 2007]. Thus, the spatial pattern of biologically mediated flux in the region is still undetermined.

[59] In this study, net air-sea CO_2 fluxes observed on spring cruises (CB1 and P16N) exhibited similar meridional trends to the climatological fluxes [*Takahashi et al.*, 2009] for April and March, respectively (Figure 9). During late–summer cruises, the net air-sea CO_2 fluxes deviated slightly from corresponding climatological averages. For CB2, a weak CO_2 sink throughout the 25°–50°N interval was observed in our study while the climatology indicates the region to be neutral or a slight CO_2 source over 25°–40°N. During STUD08, a strong ocean CO_2 sink was detected between 42°–47°N that is not present in climatology (Figure 9). Meridional trends in *NCP*, converted to a C-equivalent flux, are broadly similar to those observed for net air-sea CO_2 flux. For the two spring cruises, both the magnitude and direction of biological and net air-sea CO_2 flux are comparable, suggesting the air-sea flux is dominated by biological CO_2 drawdown in spring; for the two summer cruises the biological and air-sea CO_2 fluxes are of different magnitude (and for STUD08, a different sign), suggesting that the air-sea flux is controlled by both biological drawdown, but also the response of the surface ML to summer warming. In the absence of biological CO_2 drawdown (i.e., in an abiotic

ocean affected only by temperature seasonality), an outgassing of up to 20 mmol m^{-2} d^{-1} would be expected (Figure 9).

[60] The net biological fluxes inferred from the O_2 mass balance presented here must be stoichiometrically related to CO_2 flux, but comparisons are complicated by two factors: 1) the inherent timescales of O_2 and CO_2 air-sea gas exchange are different (approximately weekly versus yearly, respectively); 2) the net air-sea CO_2 flux is a combination of solubility-induced flux, a biologically induced flux, and a net physical flux, whereas the biological O_2 flux only tracks one of these terms. Ultimately ΔO_2:ΔCO_2 stoichiometry for biological fluxes is coupled on longer timescales – i.e., a measured surplus in O_2 would have a stoichiometrically equivalent CO_2 signature, even if the air-sea gas flux associated with this CO_2 deficit occurs over a much different timescale. However, diagnosis of biologically–induced fluxes from CO_2 is difficult because of a low signal-to-noise ratio and the sluggish response timescale noted above, which allows physical and solubility effects to convolute the signal. For example, a 10 μmol kg^{-1} change in DIC or O_2 is 0.5% and 4% of the respective surface concentration of each (10/2000 versus 10/250), while the relative detection limits are ≈0.1% (2 μmol kg^{-1} and 0.2 μmol kg^{-1}, respectively). For pCO_2, the signal would be comparable to O_2 (5%, or 20 μatm assuming a Revelle factor of 10), but the noise (2–3 μatm [*Pierrot et al.*, 2009]) is still a higher proportion of the signal compared to O_2.

6.2. Modeled Carbon Budget

[61] To illustrate the seasonality in the individual components of net air-sea CO_2 flux (physical supply, solubility changes, and net organic carbon production) we modeled surface carbon inventory changes using the most recently published air-sea CO_2 flux climatology [*Takahashi et al.*, 2009] and a simplified version of the approach of *Lee* [2001]. Briefly, surface pCO_2, sea surface temperature and salinity from the 2009 climatology and TA calculated from *Lee et al.* [2006] were used to determine a salinity–normalized DIC for each month, and each 4° (latitude) × 5° (longitude) climatology box between 24°N and 48°N. A DIC budget was constructed with terms for the time-rate of change of DIC ($\frac{\partial DIC}{\partial t}$), air-sea CO_2 exchange ($k_{CO2}\Delta pCO_2$), *NCP*, and physical fluxes

$$h\frac{\partial DIC}{\partial t} = k_{CO2}\Delta pCO_2 + NCP + Physics, \qquad (6)$$

where $k_{CO2}\Delta pCO_2$ includes the temperature and salinity dependent gas transfer coefficient for CO_2 (k_{CO2}) and the air-sea gradient of pCO_2, i.e., $\Delta pCO_2 = pCO_{2,atm} - pCO_{2,w}$ determined from the 2009 climatology. The $\frac{\partial DIC}{\partial t}$ was calculated for each month, and the observed monthly air-sea CO_2 flux subtracted to solve for an "*NCP + Physics*" term. We group the *NCP* and *Physics* flux terms because determining the time-dependent net physical supply for each climatological box would be an involved effort (indeed, this is the focus of a recent paper [*Ayers and Lozier*, 2012]), and our purpose here is to provide a simple illustration of the seasonal controls on the carbon budget . To a first approximation, in summer, we would expect the physical contributions to the DIC budget to be minimized [*Lee*, 2001; *Quay and Stutsman*, 2003; *Ayers and Lozier*, 2012], and this term to be a reasonable estimate of *NCP*. In winter, the DIC budget is driven by physical transport and air-sea gas exchange, and thus the *NCP+Physics* term approximates *Physics*, rather than *NCP*. For a more detailed investigation of the physical control on DIC inventory on a seasonal basis, we direct the reader to the more comprehensive model presented in *Ayers and Lozier* [2012].

[62] The seasonal cycle in surface temperature, air and seawater pCO_2, modeled DIC, and modeled rate terms in equation (6) is shown in Figure 10 for selected climatological boxes. Two points are immediately illustrated by this exercise: (1) the inventory change in DIC is dominated by the *NCP+Physics* term, and (2) a substantial DIC removal (*NCP*) is predicted over spring and summer throughout the N. Pacific basin. Integrations of the shaded gray area, the carbon drawdown indicated by the *NCP+Physics* term, are given in mmol m^{-2} at the bottom of each box, and values for all climatological boxes between 24°N and 48°N are shown in Figure 10e. The simplified DIC budget yields *NCP* estimates of ≈1.5 mol C m^{-2} for 24°–40°N, and a twofold increase at the northern boundary of the transition region, between 40°–45°N. While the carbon-budget estimate of *NCP* for the subarctic region (2.0 mol m^{-2}) agrees quite well with that determined in this and previous studies (Table 2), the *NCP* predicted for the subtropics (1.4 mol m^{-2}) is substantially lower than has been determined from independent estimates [*Quay and Stutsman*, 2003; *Emerson et al.*, 2008], and our own work. This may in part be due to the assumption that physical transport is zero (i.e., *NCP+Physics* ≈ *NCP*). *Quay and Stutsman* [2003] determined the net physical transport (vertical mixing + advection) during summer at HOT was +0.7 mmol C m^{-2} d^{-1}; a correction for this physical DIC supply would raise calculated estimates of *NCP* only modestly (≈0.2 mol C m^{-2}). Additional *NCP* in fall and winter periods (which have been excluded in our integrations because of difficulty in separating from physical supply) may help explain the remaining discrepancy, since *NCP* has been shown to be positive year-round at HOT [e.g., *Hamme and Emerson*, 2006; *Emerson et al.*, 2008]. Carbon-based estimates of *NCP* are also about 1.5 mol m^{-2} lower than the observed, $\Delta O_2/Ar$–based mean rates through the majority of the transition region (30°–40°N, Table 2 and Figure 10), but potential causes of this discrepancy are unclear. *Ayers and Lozier* [2012] report that the net effect of physical processes is a modest DIC removal (7 μatm mo^{-1} removal of pCO_2 in summer, which corresponds to a ΔDIC of ≈−0.7 mmol C m^{-3} mo^{-1} assuming a Revelle factor of 10). This removal would decrease calculated *NCP* slightly (≈0.3 mol C m^{-2}, for a z_{ML} = 50 m over 9 months). While additional *NCP* in fall and winter, not accounted for in the simplified carbon budget presented here, may be able to account for a small amount of the difference between the carbon model and observations, it is hard to imagine it would contribute the amount required to bring the two into agreement (1.5 mol m^{-2}) . Clearly further examination of the annual biologically induced air-sea CO_2 flux is needed in this region.

[63] Regardless of discrepancies with observations, these simple carbon budget calculations demonstrate that the seasonal, biologically mediated DIC removal (1.5–3 mol m^{-2} for 25°N–45°N, Figure 10) is an important term contributing to the net annual air-sea CO_2 flux in the NE Pacific (0.8–2 mol m^{-2};

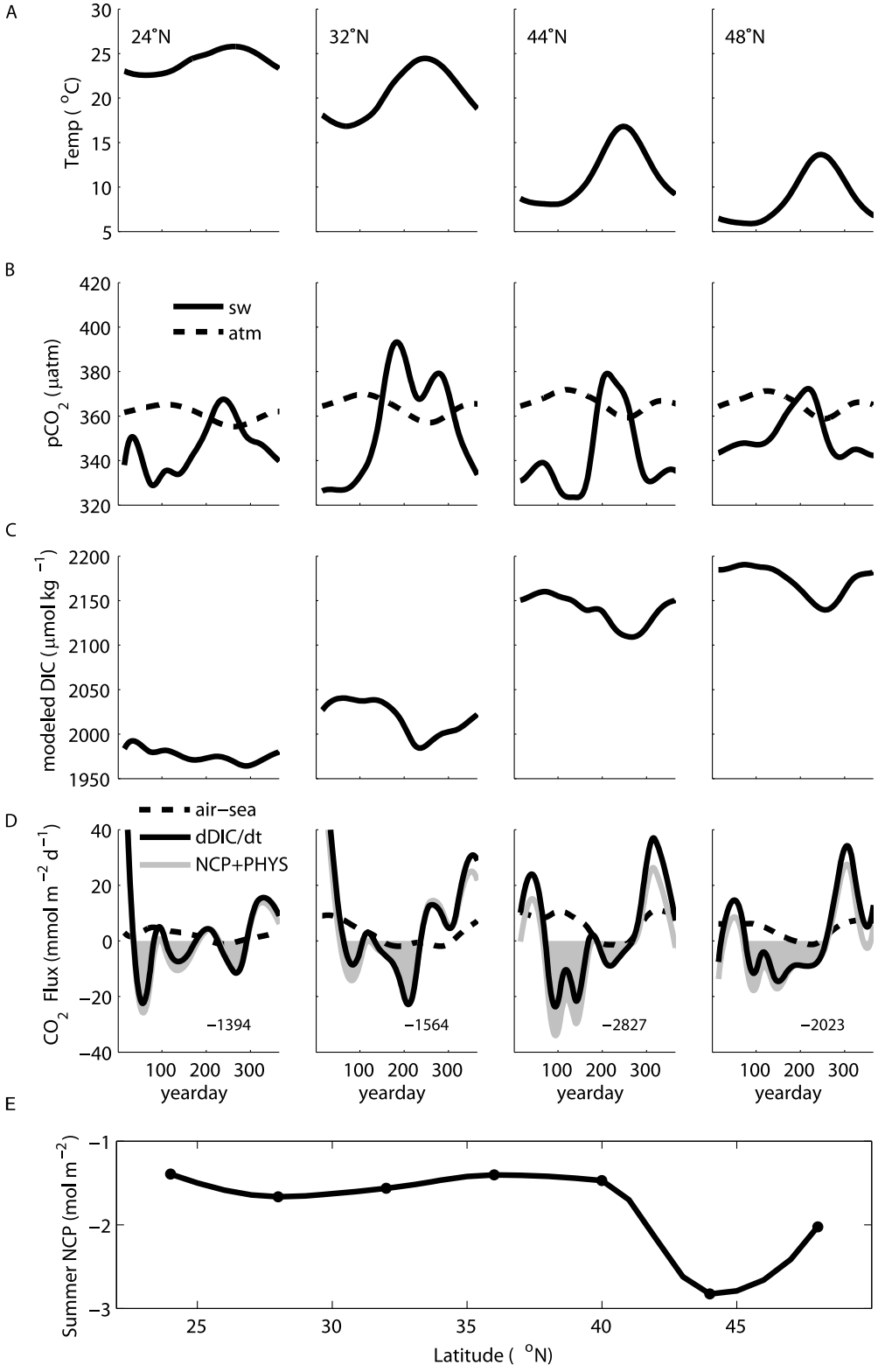

Figure 10. Modeled carbon budget for selected pCO_2 climatology boxes along 152°W. (a and b) The seasonal cycle of temperature, $pCO_{2,w}$ and $pCO_{2,a}$ from the *Takahashi et al.* [2009] climatology. (c and d) The modeled DIC inventory and individual flux terms. Numbers in lower right corner of the Figure 10d plots indicate an integration of the gray shaded area (i.e., the calculated *NCP* if physical supply/removal of DIC is presumed to be negligible). (e) The result of the same integration for all boxes between 24°N and 48°N.

Table 2). Because the previously discussed signal:noise issues, and the convoluting effects of solubility and physics over a longer air-sea equilibration timescale tend to obscure the importance of biological CO_2 flux, this may not be well-recognized. Thus, there is clear need to further evaluate mechanisms controlling biological carbon cycling and the importance of the biologically mediated CO_2 flux throughout the N. Pacific region.

7. Conclusions

[64] We report here regionally averaged rates of *GOP* and *NCP* (Table 1 and Figure 7) for two spring and two late summer/early fall cruises in the NE Pacific basin. Observed *GOP* and *NCP* in the subtropical (89 ± 9 and 8.3 ± 1.3 mmol O_2 m^{-2} d^{-1}, respectively) and subarctic (193 ± 16 and 16.3 ± 3.8 mmol O_2 m^{-2} d^{-1}) were in agreement with rates previously determined at time series stations in each region, validating the regional representativeness of these sites. We have also demonstrated that a convergence of physical, chemical, and biological forcing in the transition region between the subtropical and subarctic N. Pacific, and more specifically, the TZCF, results in significant enhancements in biological productivity and *NCP*. The role of certain phytoplankton taxa in contributing to enhanced biological activity needs to be further evaluated, but the evidence presented here indicates that diatoms and coccolithophores may play primary roles. Climate-induced changes in hydrography, whether by modes of natural variability (e.g., ENSO, PDO) or anthropogenic forcing, may result in changes in community structure and hence, biological production and export near the TZCF. Regardless, without a longer time series of observations under a range of conditions it will be impossible to predict any impacts of large scale climate phenomena on biological carbon cycling in the region.

[65] Analysis of short-term and seasonal timescale air-sea CO_2 flux from this study and the *Takahashi et al.* [2009] climatology indicates that biologically–regulated CO_2 flux is a first order term driving annual net CO_2 uptake. However, its importance may be obscured by the long timescale associated with air-sea CO_2 equilibration. A better understanding of biological pump contribution to the net air-sea CO_2 flux and potential coupled climate- biosphere feedbacks is therefore essential for constraint on future ocean CO_2 uptake in this important region.

[66] **Acknowledgments.** The authors thank the many scientists and ships' crew who supported this work with collection and processing of ancillary chemical, biological, and hydrographic data in the field. D. Wilbur, J. Stutsman, and M. Haught provided invaluable help with the isotopic analyses. We also thank the NASA Ocean Color Working Group for making gridded estimates of remotely sensed chl and PIC freely available. This work was supported by a NASA ESS Graduate Fellowship and NOAA GCC NA10OAR4310090 (LWJ) and was funded in part by National Science Foundation grant EF-0424599 and the Gordon and Betty Moore Foundation (DMK). This work was also partially funded by the Joint Institute for the Study of Atmosphere and Ocean (JISAO) under NOAA Cooperative agreements NA17RJ1232 and NA10OAR4320148, contribution 1878, and NOAA PMEL contribution 3726.

References

Angert, A., S. Rachmilevitch, E. Barkan, and B. Luz (2003), Effects of photorespiration, the cytochrome pathway, and the alternative pathway on the triple isotopic composition of O_2, *Global Biogeochem. Cycles*, *17*(1), 1030, doi:10.1029/2002GB001933.

Ayers, J., and M. S. Lozier (2010), Physical controls on the seasonal migration of the North Pacific transition zone chlorophyll front, *J. Geophys. Res.*, *115*, C05001, doi:10.1029/2009JC005596.

Ayers, J., and M. S. Lozier (2012), Unraveling dynamical controls on the North Pacific carbon sink, *J. Geophys. Res.*, *117*, C01017, doi:10.1029/2011JC007368.

Balch, W. M., H. R. Gordon, B. C. Bowler, D. T. Drapeau, and E. S. Booth (2005), Calcium carbonate measurements in the surface global ocean based on Moderate-Resolution Imaging Spectroradiometer data, *J. Geophys. Res.*, *110*, C07001, doi:10.1029/2004JC002560.

Behrenfeld, M. J., and P. G. Falkowski (1997), Photosynthetic rates derived from satellite-based chlorophyll concentration, *Limnol. Oceanogr.*, *42*(1), 1–20, doi:10.4319/lo.1997.42.1.0001.

Benitez-Nelson, C., K. O. Buesseler, D. M. Karl, and J. Andrews (2001), A time-series study of particulate matter export in the North Pacific Subtropical Gyre based on ^{234}Th:^{238}U disequilibrium, *Deep Sea Res., Part I*, *48*, 2595–2611, doi:10.1016/S0967-0637(01)00032-2.

Bond, N. A., and D. E. Harrison (2000), The Pacific Decadal Oscillation, air-sea interaction and central north Pacific winter atmospheric regimes, *Geophys. Res. Lett.*, *27*(5), 731–734, doi:10.1029/1999GL010847.

Boyd, P., and S. Doney (2002), Modelling regional responses by marine pelagic ecosystems to global climate change, *Geophys. Res. Lett.*, *29*(15), 1806, doi:10.1029/2001GL014130.

Boyd, P., and P. J. Harrison (1999), Phytoplankton dynamics in the NE subarctic Pacific, *Deep Sea Res., Part II*, *46*, 2405–2432, doi:10.1016/S0967-0645(99)00069-7.

Boyd, P. W., F. A. Whitney, P. J. Harrison, and C. S. Wong (1995), The NE subarctic Pacific in winter: Part II. Biological rate processes, *Mar. Ecol. Prog. Ser.*, *128*, 25–34, doi:10.3354/meps128025.

Brix, H., N. Gruber, D. Karl, and N. Bates (2006), On the relationships between primary, net community, and export production in subtropical gyres, *Deep Sea Res., Part II*, *53*, 698–717, doi:10.1016/j.dsr2.2006.01.024.

Chai, F., M. Jiang, R. T. Barber, R. C. Dugdale, and Y. Chao (2003), Interdecadal variation of the transition zone chlorophyll front: A physical-biological model simulation between 1960–1990, *J. Oceanogr.*, *59*, 461–475, doi:10.1023/A:1025540632491.

Charette, M. A., S. B. Moran, and J. K. Bishop (1999), ^{234}Th as a tracer of particulate organic carbon export in the subarctic northeast Pacific Ocean, *Deep Sea Res., Part II*, *46*, 2833–2861, doi:10.1016/S0967-0645(99)00085-5.

Chavez, F. P., J. Ryan, S. E. Lluch-Cota, and C. M. Ñiquen (2003), From anchovies to sardines and back: Multidecadal change in the Pacific Ocean, *Science*, *299*, 217–221, doi:10.1126/science.1075880.

Chierici, M., A. Fransson, and Y. Nojiri (2006), Biogeochemical processes as drivers of surface fCO_2 in contrasting provinces in the subarctic North Pacific Ocean, *Global Biogeochem. Cycles*, *20*, GB1009, doi:10.1029/2004GB002356.

Church, M. J., C. M. Short, B. D. Jenkins, D. M. Karl, and J. P. Zehr (2005), Temporal patterns of nitogenase gene (*nif* H) expression in the oligotrophic North Pacific Ocean, *Appl. Environ. Microbiol.*, *71*, 5362–5370, doi:10.1128/AEM.71.9.5362-5370.2005.

Church, M., K. Bjorkman, D. Karl, M. Saito, and J. Zehr (2008), Regional distributions of nitrogen-fixing bacteria in the Pacific Ocean, *Limnol. Oceanogr.*, *53*(1), 63–77, doi:10.4319/lo.2008.53.1.0063.

Corno, G., D. Karl, M. Church, R. Letelier, R. Lukas, R. Bidigare, and M. Abbott (2007), Impact of climate forcing on ecosystem processes in the North Pacific Subtropical Gyre, *J. Geophys. Res.*, *112*, C04021, doi:10.1029/2006JC003730.

Craig, H., and T. L. Hayward (1987), Oxygen supersaturation in the ocean: Biological versus physical contributions, *Science*, *235*, 199–202, doi:10.1126/science.235.4785.199.

Denman, K. L., C. Voelker, M. A. Peña, and R. B. Rivkin (2006), Modelling the ecosystem response to iron fertilization in the subarctic NE Pacific: The influence of grazing, and Si and N cycling on CO_2 drawdown, *Deep Sea Res., Part II*, *53*, 2327–2352, doi:10.1016/j.dsr2.2006.05.026.

Dickson, A. G., C. L. Sabine, and J. R. Christian (Eds.) (2007), Guide to best practices for ocean CO_2 measurements, *PICES Spec. Publ. 3*, 191 pp., N. Pac. Mar. Sci. Organ., Sidney, B. C., Canada.

Dore, J., R. Lukas, D. Sadler, and D. Karl (2003), Climate-driven changes to the atmospheric CO2 sink in the subtropical North Pacific Ocean, *Nature*, *424*, 754–757, doi:10.1038/nature01885.

Eisenstadt, D., E. Barkan, B. Luz, and A. Kaplan (2010), Enrichment of oxygen heavy isotopes during photosynthesis in plankton, *Photosynth. Res.*, *103*(2), 97–103, doi:10.1007/s11120-009-9518-z.

Emerson, S. (1987), Seasonal oxygen cycles and biological new production in surface waters of the subarctic Pacific Ocean, *J. Geophys. Res.*, *92*, 6535–6544, doi:10.1029/JC092iC06p06535.

Emerson, S., and C. Stump (2010), Net biological oxygen production in the ocean-II: Remote in situ measurements of O_2 and N_2 in subarctic Pacific

surface waters, *Deep Sea Res., Part I*, *57*, 1255–1265, doi:10.1016/j.dsr.2010.06.001.

Emerson, S., P. D. Quay, C. Stump, D. Wilbur, and M. Knox (1991), O_2, Ar, N_2, and ^{222}Rn in surface waters of the subarctic ocean: Net biological O_2 production, *Global Biogeochem. Cycles*, *5*, 49–69, doi:10.1029/90GB02656.

Emerson, S., P. Quay, D. Karl, C. Winn, L. Tupas, and M. Landry (1997), Experimental determination of the organic carbon flux from open-ocean surface waters, *Nature*, *389*, 951–954, doi:10.1038/40111.

Emerson, S., C. Stump, D. Wilbur, and P. Quay (1999), Accurate measurement of O_2, N_2, and Ar gases in water and the solubility of N_2, *Mar. Chem.*, *64*, 337–347, doi:10.1016/S0304-4203(98)00090-5.

Emerson, S., C. Stump, and D. Nicholson (2008), Net biological oxygen production in the ocean: Remote in situ measurements of O_2 and N_2 in surface waters, *Global Biogeochem. Cycles*, *22*, GB3023, doi:10.1029/2007GB003095.

Eppley, R. W., and B. W. Peterson (1979), Particulate organic matter flux and planktonic new production in the deep ocean, *Nature*, *282*, 677–680, doi:10.1038/282677a0.

García, H. E., and L. I. Gordon (1992), Oxygen solubility in seawater: Better fitting equations, *Limnol. Oceanogr.*, *37*, 1307–1312, doi:10.4319/lo.1992.37.6.1307.

Glover, D. M., J. S. Wroblewski, and C. R. McClain (1994), Dynamics of the transition zone in coastal zone color scanner –sensed ocean color in the North Pacific during oceanographic spring, *J. Geophys. Res.*, *99*(C4), 7501–7511, doi:10.1029/93JC02144.

Gruber, N., et al. (2009), Oceanic sources, sinks, and transport of atmospheric CO_2, *Global Biogeochem. Cycles*, *23*, GB1005, doi:10.1029/2008GB003349.

Halsey, K., A. Milligan, and M. Behrenfeld (2010), Physiological optimization underlies growth rate-independent chlorophyll-specific gross and net primary production, *Photosynth. Res.*, *103*(2), 125–137, doi:10.1007/s11120-009-9526-z.

Hamme, R. C., and S. R. Emerson (2004), The solubility of neon, nitrogen and argon in distilled water and seawater, *Deep Sea Res. Part I*, *51*, 1517–1528.

Hamme, R. C., and S. R. Emerson (2006), Constraining bubble dynamics and mixing with dissolved gases: Implications for productivity measurements by oxygen mass balance, *J. Mar. Res.*, *64*(1), 73–95, doi:10.1357/002224006776412322.

Hamme, R., et al. (2010), Volcanic ash fuels anomalous plankton bloom in subarctic northeast Pacific, *Geophys. Res. Lett.*, *37*, L19604, doi:10.1029/2010GL044629.

Harrison, P. (2002), Station papa time series: Insights into ecosystem dynamics, *J. Oceanogr.*, *58*, 259–264, doi:10.1023/A:1015857624562.

Helman, Y., E. Barkan, D. Eisenstadt, B. Luz, and A. Kaplan (2005), Fractionation of the three stable oxygen isotopes by oxygen-producing and oxygen-consuming reactions in photosynthetic organisms, *Plant Physiol.*, *138*(4), 2292–2298, doi:10.1104.pp.105.063768.

Hendricks, M. B., M. L. Bender, and B. A. Barnett (2004), Net and gross O_2 production in the southern ocean from measurements of biological O_2 saturation and its triple isotope composition, *Deep Sea Res., Part I*, *51*, 1541–1561.

Hendricks, M. B., M. L. Bender, B. A. Barnett, P. Strutton, and F. P. Chavez (2005), Triple oxygen isotope composition of dissolved O_2 in the equatorial Pacific: A tracer of mixing, production, and respiration, *J. Geophys. Res.*, *110*, C12021, doi:10.1029/2004JC002735.

Ho, D., C. S. Law, M. J. Smith, P. Schlosser, M. Harvey, and P. Hill (2006), Measurements of air-sea gas exchange at high wind speeds in the Southern Ocean: Implications for global parameterizations, *Geophys. Res. Lett.*, *33*, L16611, doi:10.1029/2006GL026817.

Howard, E., S. Emerson, S. Bushinsky, and C. Stump (2010), The role of net community production in air-sea carbon fluxes at the North Pacific subarctic-subtropical boundary region, *Limnol. Oceanogr.*, *55*(6), 2585–2596, doi:10.4319/lo.2010.55.6.2585.

Johnson, K., S. Riser, and D. Karl (2010), Nitrate supply from deep to near-surface waters of the North Pacific subtropical gyre, *Nature*, *465*, 1062–1065, doi:10.1038/nature09170.

Juranek, L. W. (2007), Assessment of Pacific Ocean organic carbon production and export using measurements of dissolved oxygen isotopes and oxygen/argon gas ratios, Ph.D. dissertation, Univ. of Wash., Seattle.

Juranek, L. W., and P. D. Quay (2005), In vitro and in situ gross primary and net community production in the North Pacific Subtropical Gyre using labeled and natural abundance isotopes of dissolved O_2, *Global Biogeochem. Cycles*, *19*, GB3009, doi:10.1029/2004GB002384.

Juranek, L. W., and P. D. Quay (2010), Basin-wide photosynthetic production rates in the subtropical and tropical Pacific Ocean determined from dissolved oxygen isotope ratio measurements, *Global Biogeochem. Cycles*, *24*, GB2006, doi:10.1029/2009GB003492.

Kaiser, J. (2011), Technical note: Consistent calculation of aquatic gross production from oxygen triple isotope measurements, *Biogeosciences*, *8*, 1793–1811, doi:10.5194/bg-8-1793-2011.

Kaiser, J., M. K. Reuer, B. Barnett, and M. L. Bender (2005), Marine productivity estimates from continuous O_2/Ar ratio measurements by membrane inlet mass spectrometry, *Geophys. Res. Lett.*, *32*, L19605, doi:10.1029/2005GL023459.

Karl, D. M. (1999), A sea of change: Biogeochemical variability in the North Pacific subtropical gyre, *Ecosystems*, *2*, 181–214, doi:10.1007/s100219900068.

Karl, D. M., and R. Letelier (2008), Nitrogen fixation-enhanced carbon sequestration in low nitrate, low chlorophyll seascapes, *Mar. Ecol. Prog. Ser.*, *364*, 257–268, doi:10.3354/meps07547.

Karl, D. M., R. Letelier, L. Tupas, J. Dore, J. Christian, and D. Hebel (1997), The role of nitrogen fixation in biogeochemical cycling in the subtropical North Pacific Ocean, *Nature*, *388*, 533–538, doi:10.1038/41474.

Karl, D. M., R. R. Bidigare, and R. M. Letelier (2001), Long-term changes in plankton community structure and productivity in the subtropical North Pacific Ocean: The domain shift hypothesis, *Deep Sea Res., Part II*, *48*, 1449–1470, doi:10.1016/S0967-0645(00)00149-1.

Keeling, C. D., H. Brix, and N. Gruber (2004), Seasonal and long-term dynamics of the upper ocean carbon cycle at Station ALOHA near Hawaii, *Global Biogeochem. Cycles*, *18*, GB4006, doi:10.1029/2004GB002227.

Lam, P. J., J. K. B. Bishop, C. C. Henning, M. A. Marcus, G. A. Waychunas, and I. Y. Fung (2006), Wintertime phytoplankton bloom in the subarctic Pacific supported by continental margin iron, *Global Biogeochem. Cycles*, *20*, GB1006, doi:10.1029/2005GB002557.

Lämmerzahl, P., T. Röckmann, C. A. M. Brenninkmeijer, D. Krankowsky, and K. Mauersberger (2002), Oxygen isotope composition of stratospheric carbon dioxide, *Geophys. Res. Lett.*, *29*(12), 1582, doi:10.1029/2001GL014343.

Laws, E. A. (1991), Photosynthetic quotients, new production and net community production in the open ocean, *Deep Sea Res., Part A*, *38*(1), 143–167, doi:10.1016/0198-0149(91)90059-O.

Laws, E. A., P. G. Falkowski, W. O. Smith Jr., H. Ducklow, and J. J. McCarthy (2000), Temperature effects on export production in the open ocean, *Global Biogeochem. Cycles*, *14*(4), 1231–1246, doi:10.1029/1999GB001229.

Lee, K. (2001), Global net community production estimated from the annual cycle of surface water total dissolved inorganic carbon, *Limnol. Oceanogr.*, *46*(6), 1287–1297, doi:10.4319/lo.2001.46.6.1287.

Lee, K., L. T. Tong, F. J. Millero, C. L. Sabine, A. G. Dickson, C. Goyet, G.-H. Park, R. Wanninkhof, R. A. Feely, and R. M. Key (2006), Global relationships of total alkalinity with salinity and temperature in surface waters of the world's oceans, *Geophys. Res. Lett.*, *33*, L19605, doi:10.1029/2006GL027207.

Le Quere, C., et al. (2005), Ecosystem dynamics based on plankton functional types for global ocean biogeochemistry models, *Global Change Biol.*, *11*, 2016–2040, doi:10.1111/j.1365-2486.2005.01004.x.

Luz, B., and E. Barkan (2000), Assessment of oceanic productivity with the triple-isotope composition of dissolved oxygen, *Science*, *288*, 2028–2031, doi:10.1126/science.288.5473.2028.

Luz, B., and E. Barkan (2005), The isotopic ratios of $^{17}O/^{16}O$ and $^{18}O/^{16}O$ in molecular oxygen and their significance in biogeochemistry, *Geochim. Cosmochim. Acta*, *69*(5), 1099–1110, doi:10.1016/j.gca.2004.09.001.

Luz, B., and E. Barkan (2009), Net and gross oxygen production from O_2/Ar, $^{17}O/^{16}O$ and $^{18}O/^{16}O$ ratios, *Aquat. Microb. Ecol.*, *56*, 133–145, doi:10.3354/ame01296.

Luz, B., and E. Barkan (2011), Proper estimation of marine gross O_2 production with $^{17}O/^{16}O$ and $^{18}O/^{16}O$ ratios of dissolved O_2, *Geophys. Res. Lett.*, *38*, L19606, doi:10.1029/2011GL049138.

Luz, B., E. Barkan, Y. Sagi, and Y. Z. Yacobi (2002), Evaluation of community respiratory mechanisms with oxygen isotopes: a case study in Lake Kinneret, *Limnol. Oceanogr.*, *47*, 33–42, doi:10.4319/lo.2002.47.1.0033.

Mantua, N., and S. Hare (2002), The Pacific Decadal Oscillation, *J. Oceanogr.*, *58*, 35–44, doi:10.1023/A:1015820616384.

Marra, J. (2002), Approaches to the measurement of plankton production, in *Phytoplankton Productivity and Carbon Assimilation in Marine and Freshwater Ecosystems*, edited by P. J. Williams, D. R. Thomas, and C. S. Reynolds, pp. 78–108, Blackwell, London, doi:10.1002/9780470995204.ch4.

Marra, J., and R. T. Barber (2004), Phytoplankton and heterotrophic respiration in the surface layer of the ocean, *Geophys. Res. Lett.*, *31*, L09314, doi:10.1029/2004GL019664.

McKinley, G. A., et al. (2006), North Pacific carbon cycle response to climate variability on seasonal to decadal timescales, *J. Geophys. Res.*, *111*, C07S06, doi:10.1029/2005JC003173.

Monterey, G., and S. Levitus (1997), *Seasonal Variability of Mixed Layer Depth for the World Ocean*, *NOAA Atlas NESDIS*, vol. 14, 96 pp., NOAA, Silver Spring, Md.

Munk, W. (1950), On the wind-driven ocean circulation, *J. Meteorol.*, *7*, 80–93, doi:10.1175/1520-0469(1950)007<0080:OTWDOC>2.0.CO;2.

Nicholson, D. (2011), Comment on: "Technical note: Consistent calculation of aquatic gross production from oxygen triple isotope measurements" by Kaiser (2011), *Biogeosciences*, *8*, 2993–2997, doi:10.5194/bg-8-2993-2011.

Nicholson, D., R. H. R. Stanley, E. Barkan, D. M. Karl, B. Luz, P. D. Quay, and S. C. Doney (2012), Evaluating triple oxygen isotope estimates of gross primary production at the Hawaii Ocean Time-series and Bermuda Atlantic Time-series Study sites, *J. Geophys. Res.*, doi:10.1029/2010JC006856, in press.

Nightingale, P. D., G. Malin, C. S. Law, A. J. Watson, P. S. Liss, M. I. Liddicoat, J. Boutin, and R. C. Upstill-Goddard (2000), In situ evaluation of air-sea exchange parameterizations using novel conservative and volatile tracers, *Global Biogeochem. Cycles*, *14*(1), 373–387, doi:10.1029/1999GB900091.

Painter, S., A. Poulton, J. Allen, R. Pidcock, and W. Balch (2010), The COPAS'08 expedition to the Patagonian Shelf Physical and environmental conditions during the 2008 coccolithophore bloom, *Cont. Shelf Res.*, *30*, 1907–1923, doi:10.1016/j.csr.2010.08.013.

Pierrot, D., C. Neill, K. Sullivan, R. Castle, R. Wanninkhof, H. Luger, T. Johannessen, A. Olsen, R. Feely, and C. Cosca (2009), Recommendations for autonomous underway pCO_2 measuring systems and data-reduction routines, *Deep Sea Res., Part II*, *56*, 512–522, doi:10.1016/j.dsr2.2008.12.005.

Polovina, J., G. Mitchum, and G. Evans (1995), Decadal and basin-scale variation in mixed layer depth and the impact on biological production in the central and North Pacific, 1960–88, *Deep Sea Res., Part I*, *42*(10), 1701–1716, doi:10.1016/0967-0637(95)00075-H.

Polovina, J., E. Howell, D. Kobayashi, and M. Seki (2001), The transition zone chlorophyll front, a dynamic global feature defining migration and forage habitat for marine resources, *Prog. Oceanogr.*, *49*, 469–483, doi:10.1016/S0079-6611(01)00036-2.

Polovina, J., F. Chai, E. Howell, D. Kobayashi, L. Shi, and Y. Chao (2008), Ecosystem dynamics at a productivity gradient: A study of the lower trophic dynamics around the northern atolls in the Hawaiian Archipelago, *Prog. Oceanogr.*, *77*, 217–224, doi:10.1016/j.pocean.2008.03.011.

Prokopenko, M. G., O. M. Pauluis, J. Granger, and L. Y. Yeung (2011), Exact evaluation of gross photosynthetic production from the oxygen triple-isotope composition of O_2: Implications for the net-to-gross primary production ratios, *Geophys. Res. Lett.*, *38*, L14603, doi:10.1029/2011GL047652.

Quay, P., and J. Stutsman (2003), Surface layer carbon budget for the subtropical N. Pacific: $\delta^{13}C$ constraints at station ALOHA, *Deep Sea Res., Part I*, *50*, 1045–1061, doi:10.1016/S0967-0637(03)00116-X.

Quay, P. D., C. Peacock, K. Bjorkman, and D. M. Karl (2010), Measuring primary production rates in the ocean: Enigmatic results between incubation and non-incubation methods at Station ALOHA, *Global Biogeochem. Cycles*, *24*, GB3014, doi:10.1029/2009GB003665.

Reuer, M. K., B. A. Barnett, M. L. Bender, P. G. Falkowski, and M. B. Hendricks (2007), New estimates of Southern Ocean biological production rates from O_2/Ar ratios and the triple isotope composition of O_2, *Deep Sea Res., Part I*, *54*, 951–974, doi:10.1016/j.dsr.2007.02.007.

Rocap, G., et al. (2003), Genome divergence in two Prochlorococcus ecotypes reflects oceanic niche differentiation, *Nature*, *424*, 1042–1047, doi:10.1038/nature01947.

Roden, G. I. (1980), On the subtropical frontal zone north of Hawaii during winter, *J. Phys. Oceanogr.*, *10*, 342–362, doi:10.1175/1520-0485(1980)010<0342:OTSFZN>2.0.CO;2.

Roden, G. I. (1991), Subarctic-subtropical transition zone of the North Pacific: Large-scale aspects and mesoscale structure, in *Biology, Oceanography, and Fisheries of the North Pacific Transition Zone and Subarctic Frontal Zone , NOAA Tech. Rep. NMFS*, vol. 105, pp. 1–38, edited by J. Wetherall, NOAA, Silver Spring, Md.

Sarma, V. V. S. S., O. Abe, N. Yoshida, and T. Saino (2006), Continuous shipboard sampling system for determination of triple oxygen isotopes and O_2/Ar ratio by dual inlet mass spectrometry, *Rapid Commun. Mass Spectrom.*, *20*, 3503–3508, doi:10.1002/rcm.2756.

Schlitzer, R. (2004), Export production in the equatorial and North Pacific derived from dissolved oxygen, nutrient, and carbon data, *J. Oceanogr.*, *60*, 53–62, doi:10.1023/B:JOCE.0000038318.38916.e6.

Stanley, R. H. R., J. B. Kirkpatrick, N. Cassar, and B. A. Barnett (2010), Net community production and gross primary production rates in the western equatorial Pacific, *Global Biogeochem. Cycles*, *24*, GB4001, doi:10.1029/2009GB003651.

Steiner, N., S. Vagle, K. Denman, and C. McNeil (2007), Oxygen and nitrogen cycling in the northeast Pacific—Simulations and observations at Station Papa in 2003/2004, *J. Mar. Res.*, *65*, 441–469.

Sweeney, C., E. Gloor, A. R. Jacobsen, R. M. Key, G. McKinley, J. L. Sarmiento, and R. Wanninkhof (2007), Constraining global air-sea gas exchange for CO2 using recent bomb ^{14}C measurements, *Global Biogeochem. Cycles*, *21*, GB2015, doi:10.1029/2006GB002784.

Takahashi, T., et al. (2002), Global sea-air CO_2 flux based on climatological surface ocean pCO_2 and seasonal biological and temperature effects, *Deep Sea Res., Part II*, *49*, 1601–1622, doi:10.1016/S0967-0645(02)00003-6.

Takahashi, T., et al. (2009), Climatological mean and decadal change in surface ocean pCO2, and net sea-air CO_2 flux over the oceans, *Deep Sea Res., Part II*, *56*, 554–577, doi:10.1016/j.dsr2.2008.12.009.

Welschmeyer, N. A., S. Strom, R. Goericke, G. DiTullio, M. Belvin, and W. Petersen (1993), Primary production in the subarctic Pacific Ocean: Project SUPER, *Prog. Oceanogr.*, *32*, 101–135, doi:10.1016/0079-6611(93)90010-B.

Westberry, T., M. Behrenfeld, D. Siegel, and E. Boss (2008), Carbon-based primary productivity modeling with vertically resolved photoacclimation, *Global Biogeochem. Cycles*, *22*, GB2024, doi:10.1029/2007GB003078.

Whitney, F. A., W. R. Crawford, and P. J. Harrison (2005), Physical processes that enhance nutrient transport and primary productivity in the coastal and open ocean of the subarctic NE Pacific, *Deep Sea Res., Part II*, *52*, 681–706, doi:10.1016/j.dsr2.2004.12.023.

Wong, C. S., F. A. Whitney, K. Iseki, J. S. Page, and J. Zeng (1995), Analysis of trends in primary productivity and chlorophyll-a over two decades at Ocean Station P (50°N, 145°W) in the subarctic Northeast Pacific Ocean, *Can. J. Fish. Aquat. Sci.*, *121*, 107–117.

Wong, C. S., N. A. D. Waser, Y. Nojiri, F. A. Whitney, J. S. Page, and J. Zeng (2002), Seasonal cycles of nutrients and dissolved inorganic carbon at high and mid latitudes in the North Pacific Ocean during the Skaugran cruises: Determination of new production and nutrient uptake ratios, *Deep Sea Res., Part II*, *49*(24–25), 5317–5338, doi:10.1016/S0967-0645(02)00193-5.